5-2013

Passive and Actuated Grasping Using Superelastic Materials for Surgical Applications

Alan M. Goyzueta
University of Nebraska-Lincoln, alangoyzueta@gmail.com

Passive and Actuated Grasping Using Superelastic Materials for Surgical Applications

by

Alan M. Goyzueta

A THESIS

Presented to the Faculty of

The Graduate College at the University of Nebraska

In Partial Fulfillment of Requirements

For the Degree of Master of Science

Major: Mechanical Engineering and Applied Mechanics

Under the Supervision of Professor Carl A. Nelson

Lincoln, Nebraska

May, 2013

Passive and Actuated Grasping Using Superelastic Materials for Surgical Applications

Alan Goyzueta, M.S.

University of Nebraska, 2013

Advisor: Carl A. Nelson

This thesis presents two devices for passive and actuated grasping for surgical applications, both using superelastic materials. The first section of the thesis discusses the design, finite element analysis, and qualitative testing of a passive retainer subassembly for a Material Handling System for Natural Orifice Translumenal Endoscopic Surgery (NOTES). The purpose of the MHS is to shuttle necessary surgical items between miniature *in vivo* robots working inside the peritoneal cavity and surgeons outside the body through a natural orifice. The retainer subassembly is part of the actual shuttle and serves the purpose of securing the items that are loaded into the shuttle for transportation. The second part of this thesis discusses the design and quantitative testing of a laparoscopic grasper with fully compliant, monolithic jaws that deform as they grasp tissue. The goal of this device was to lessen the maximum pinch forces applied to soft tissues in an effort to prevent excess tissue trauma caused by excessive grasping forces.

Acknowledgements

I would like to thank Dr. Nelson for his abundant help and guidance while I was both an undergraduate and graduate student in his lab for both of these projects. Big thanks to Jeff #2 for doing a great job on the NOTES MHS which allowed me to do the testing I needed. Also thank you to Brittany for helping out with designing and testing the grasper during the summer you were in our lab. I would also like to thank everyone in the lab that made it a great place to work for the past 3+ years: Sina, Michael, Jeff #1, Jeff #2, Mamur, Mohsen, Zhao, Tao, Chi Min, Wei Jian, Chris, Jared, and Thao. I would finally like to thank my family for supporting me during my six years of college.

Table of Contents

List of Figures

List of Tables

Chapter 1 Introduction

Reducing the invasiveness of surgery has long been a goal for medical research. Decreasing the amount of "disturbance" to the body has proved to reduce recovery time, infection risk, and post-operative pain. As a result smaller incisions are used to access the surgery sites as opposed to the more invasive approach of open surgery. In minimally invasive procedures such as laparoscopic and endoscopic surgery, a group of small incisions are made to introduce tools into the body. These tools may need to have some degree of flexibility to achieve the angles needed to effectively manipulate soft tissues or organs. Going one step further, Natural Orifice Translumenal Endoscopic Surgery (NOTES) requires no external incisions, therefore further decreasing recovery time and infection risk as well as eliminating visible scarring. For this type of procedure, surgical tools are passed through a natural orifice of the body such as the esophagus to access the peritoneal cavity. By taking this indirect approach to the surgery site, much emphasis is placed on the flexibility of the instruments needed for navigation.

This shift in approaches has created a need for a new kind of surgical tools that has flexible elements to ensure functionality in spatially constrained environments. More and more, tools used in the operating room have some kind of elastic or compliant component to help them navigate, orientate, or manipulate inside the body. In some cases a tool will need large amounts of compliance or flexibility to reach extreme angles or accommodate large items and in those instances materials with superelastic properties can be used to address those needs.

This thesis presents two devices that both use superelastic materials for passive and actuated grasping for surgical applications. The first part discusses the design, finite

element (FE) analysis, and qualitative testing of a passive retainer assembly that is part of a material handling system for NOTES. The purpose of this handling system is to shuttle necessary surgical items between miniature *in vivo* robots working inside the peritoneal cavity and surgeons outside the body through a natural orifice. The retainer assembly is part of the actual shuttle and serves the purpose of securing the items that are loaded into the shuttle for transportation. These items could be things such as suture thread, staples, robotic tool tips, and tissue retrieval bags. The second part of this thesis discusses the design and quantitative testing of a laparoscopic grasper with fully compliant, monolithic jaws that deform as they grasp tissue. The goal of this device was to lessen the maximum pinch forces applied to soft tissues in an effort to prevent excess tissue trauma caused by excessive grasping forces. Using a jaw made from superelastic materials would allow the grasper to undergo large deformations that would occur during grasping while being able to fully recover to its original form.

Chapter 2 Background

Nitinol is a metallic alloy containing a nearly 1:1 atomic ratio of nickel and titanium and was invented in the 1960s at the Naval Ordnance Laboratory by William Buehler. It was found to have special properties that were not found in common engineering materials. Properties such as superelasticity [2-1], thermally triggered shape-memory [2-2], and stress hysteresis [2-3] were all found in Nitinol which led it to be commonly classified as a shape-memory alloy (SMA) [2-4].

Nitinol was selected as the material of choice for these two projects because of its superelasticity meaning that it could experience strains up to approximately 8% [2-5, 6] and fully recover. Nitinol also has other favorable characteristics such as shape-setting capabilities [2-7] and biocompatibility [2-8, 9]. Shape-setting allows the Nitinol to be formed into a desired shape through a simple heat treatment of stock materials such as wire or ribbon while they are constrained in a fixture such as a compression die or jig. Nitinol has already been used in medical devices for both surgical tools and implanted devices [2-10].

2.1 Shape-Memory

It was explained by De Lange [2-4] that heating and cooling Nitinol or applying stress induces a solid-state phase transformation in the crystalline structure between the austenite and martensite phases. The austenite phase is present at higher temperatures and is stronger and more stable than the martensite phase, which is present at lower temperatures. When the austenite phase is rapidly cooled (quenched) from an elevated temperature it transforms immediately into the martensite phase. The degree of transformation is dependent on the transitional temperatures that dictate at what

temperatures the transformation starts and finishes between austenite and martensite [2-11]. The austenite phase is the crystalline structure the Nitinol “remembers” so after the Nitinol is deformed at low temperatures and reheated above the A_f temperature (the temperature at which the transformation to austenite has finished), it will recover back to its original shape and size in the austenitic phase.

In practice, the Nitinol is shape set by constraining it in a fixture while it is being heat treated at an elevated temperature (>500°C) and then cooled rapidly to transform the austenite into martensite. In the martensite phase, the Nitinol can then be deformed and subsequently reheated to the point where all the martensite transforms back into austenite. Macroscopically, during this reheating, the Nitinol reverts from its deformed state back to the original shape it “remembers”. This type of Nitinol is commonly referred to as “shape memory” Nitinol [2-12] and the process is illustrated in Figure 2-1. M_s and M_f indicate the temperatures where the transformation from austenite to martensite starts and finishes. Likewise A_s and A_f denote temperatures where the austenitic transformation starts and finishes.

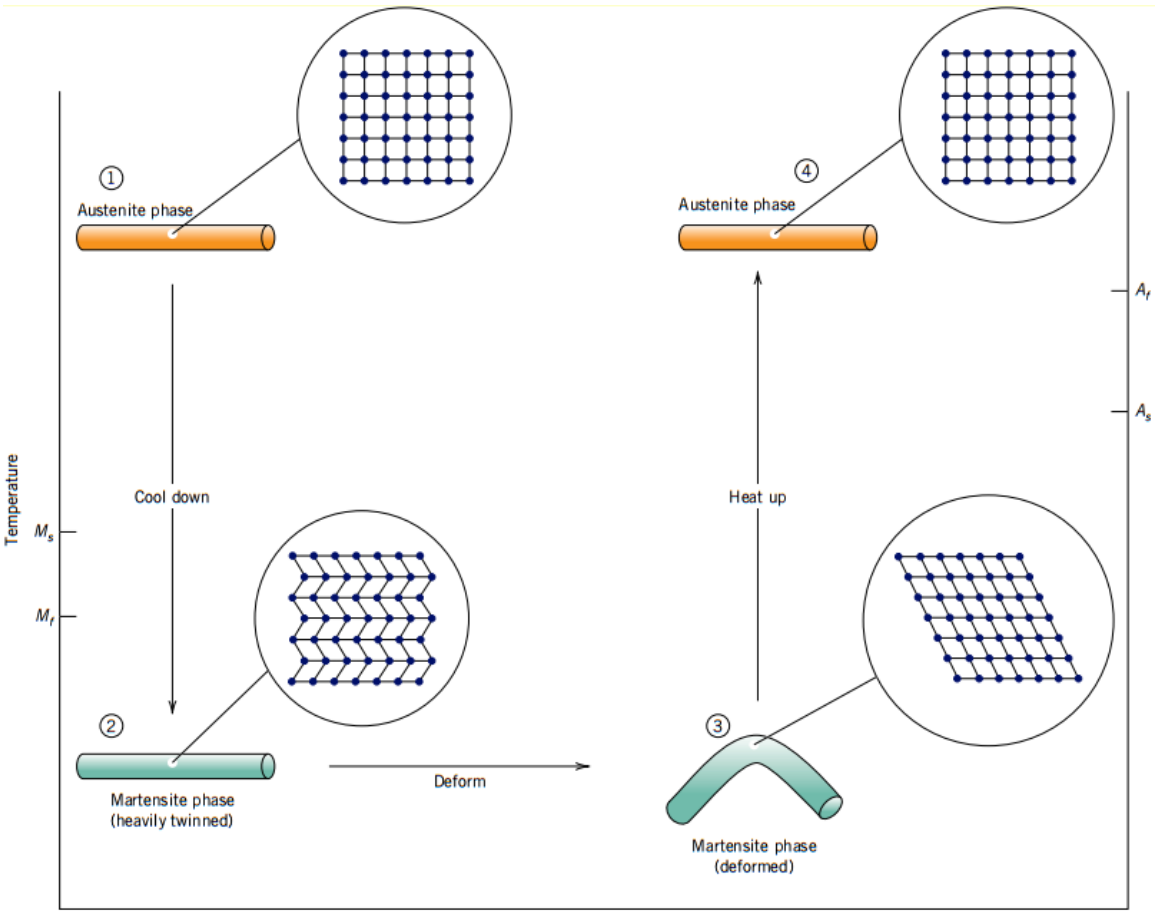

Figure 2-1 Illustration of the Thermal Shape-Memory Effect [2-11]

The shape memory effect of Nitinol can also be used mechanically. Similar to applying heat, stress can be applied to Nitinol to induce the solid-state phase transformation between austenite and martensite [2-4]. But unlike heat, stress causes the austenite to transform into martensite and once the stress is removed the martensite transforms back into austenite. This is possible by manufacturing the Nitinol so that its A_f temperature is very low (-20 – 0 °C) meaning that in ambient conditions the Nitinol will be in the austenitic phase. This is commonly referred to "superelastic" [2-12] Nitinol because the maximum fully recoverable strain can be up to 8% depending on the composition and heat treatment history. Figure 2-2 illustrates this concept.

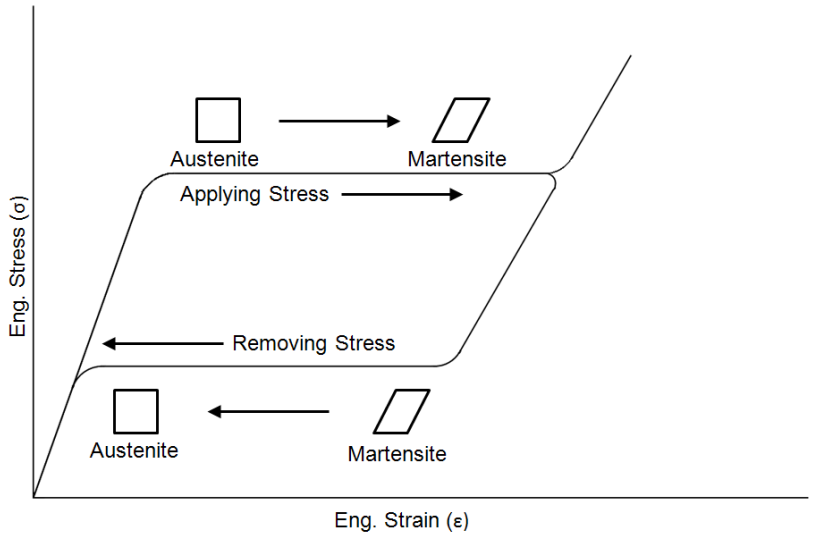

Figure 2-2 Illustration of Mechanical Shape-Memory Effects

2.2 Biocompatibility

Whenever foreign objects are introduced into the body it is required that their presence does not cause adverse reactions. Excessive exposure to nickel, one of the main constituents of Nitinol, can cause problems such as respiratory disorders, allergic reactions, and reduced cell reproduction [2-13] but titanium, on the other hand, is bioinert [2-9] and has been shown not to cause adverse reactions. Nitinol has good biocompatibility characteristics because the Ni-Ti bond is very strong, preventing the nickel ions from leaching into the body. Corrosion tests of orthodontic Nitinol wires [2-14] and clot filters using Nitinol [2-15] have shown that nickel levels in the blood are below that of a normal dietary intake after prolonged implantation. The surface of Nitinol has a titanium oxide layer that may be released by surface pitting, but these particles are ingested by phagocytes in the body, so this is not highly problematic [2-16].

2.3 Medical Applications

Nitinol has been primarily used for implant devices that take advantage of the thermal shape-memory property. Devices such as Nitinol stents used in angioplasty procedures can be heavily deformed to fit inside a catheter then introduced percutaneously to a site of vascular stenosis where they are deployed and expanded to a preset shape. By tuning the Nitinol so that its A_f transition temperature is below body temperature, the stent will expand when it is introduced to the blood stream as the deformed martensite transforms to austenite. Figure 2-3 shows the expansion process of a highly deformed Nitinol stent when the sheath is removed similar how it would in an angioplasty procedure.

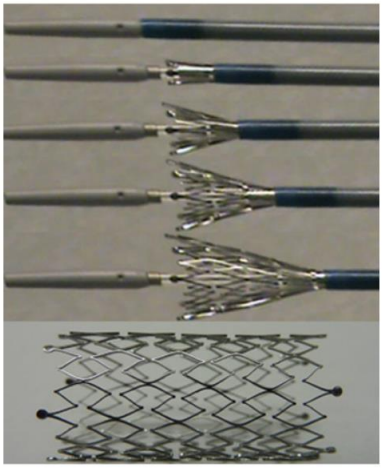

Figure 2-3 Expansion Process of Nitinol Stent [2-17]

The OPTEASE® Retrievable Vena Cava Filter (Cordis, Bridgewater, NJ) is inserted into a major vein to prevent blood clots from reaching the lungs and reducing oxygen intake in the blood stream. Like Nitinol stents the OPTEASE® uses the body heat to expand the filter to allow for easier deployment.

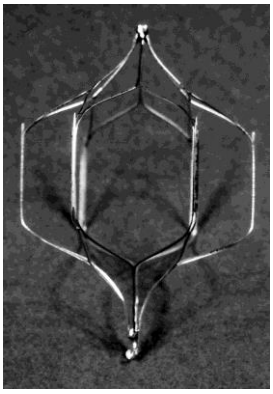

Figure 2-4 OPTEASE Vena Cava Filter [2-18]

Nitinol has also been used in surgical tools when flexibility is needed to accommodate irregular geometries. The Zerotip™ basket and Graspit™ forceps (Boston Scientific, Natick, MA) are Nitinol devices designed to aid in the retrieval and removal of stones from the renal system. The forceps and baskets can be collapsed and fed through a working channel in a flexible ureterorenoscope to access the stones for removal or repositioning so that they can be fractured into smaller pieces by either sonic impulses or holmium laser pulses and subsequently removed [2-19].

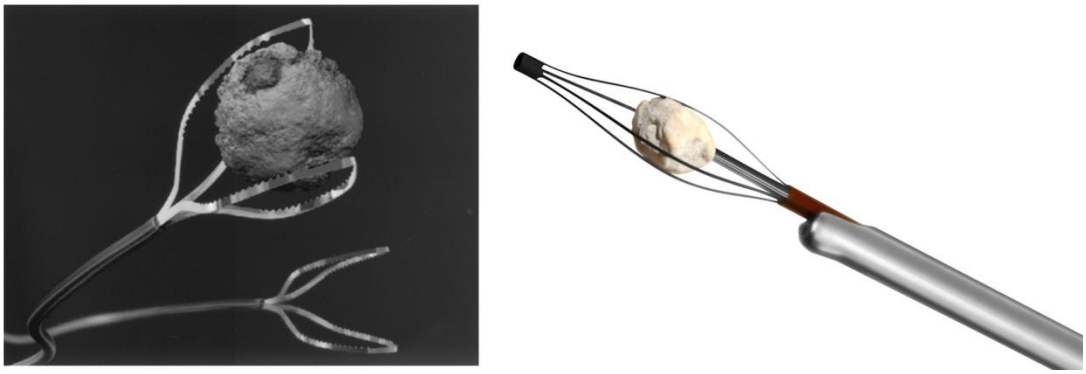

Figure 2-5 Nitinol Stone Retrieval Forceps [2-19] and Basket [2-20]

The success of these implanted devices and their demonstrations of biocompatibility show that using Nitinol for temporary surgical interventions will not be a biocompatibility concern.

These surgical devices primarily use Nitinol for some form of shape retention in their operation. In general, minimally invasive procedures require their tools to produce some kind of motion or force from a distance due to the constrained methods of introducing tools into the body through restrictive access points such as trocars. The first device presented, the NOTES retainer, uses superelastic Nitinol to grasp objects remotely from the surgeon for the purpose of material delivery. By using a superelastic material, this grasping action can be accomplished without direct control from the user, reducing the overall complexity of the device.

Chapter 3 Passive Grasping – NOTES Shuttle

3.1 Motivation

Natural Orifice Translumenal Endoscopic Surgery (NOTES) is a type of minimally invasive surgical procedure where no external incisions are made on the patient and the surgical site is accessed through the natural orifices of the body whether that be transgastric (Figure 3-1), transvaginal, or transcolonic. Benefits to the patient by accessing the peritoneal cavity through a natural orifice include a reduced risk of infection and improved recovery time [3-1]. On the other hand, accessing the surgical site through a natural lumen poses challenges to surgeons. Surgical tools need to be dexterous enough to navigate to the surgical site due to the constrained environment of the natural orifices.

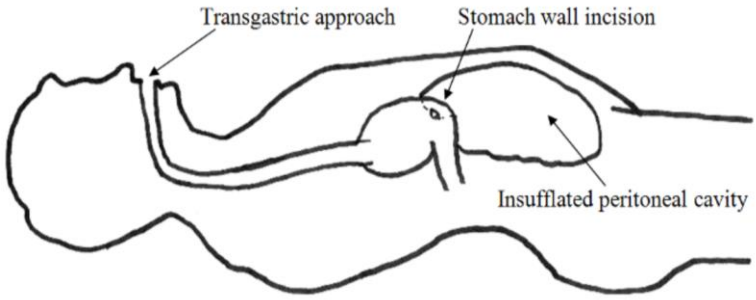

Figure 3-1 Example of Transgastric Approach for NOTES [3-2]

One solution for NOTES is the use of *in vivo* robots which can be fully inserted into the peritoneal cavity by way of a natural orifice. Some robots have been tested in porcine models and have shown promising results [3-3,4,5]. While these robots are able to operate in an insufflated peritoneal cavity, the issue of material handling becomes significant. Without external incisions and trocars to pass needed items to the robots such

as sutures, staples, other surgical tools, or excised tissue bags, another means of shuttling material between the surgeon and *in vivo* robots was needed.

A material handling system was developed [3-2] to navigate through the natural orifices to the peritoneal cavity to provide a means of transporting the aforementioned items. This system consisted of a multi-channel silicone overtube (Figure 3-2) with a helical drive spring that when rotated would move a shuttle from one end of the tube to the other much like a twist-tip mechanical pencil. This shuttle was intended to act as a vehicle of transporting the needed items from the surgeon to the *in vivo* robots or from the robots to the surgeon.

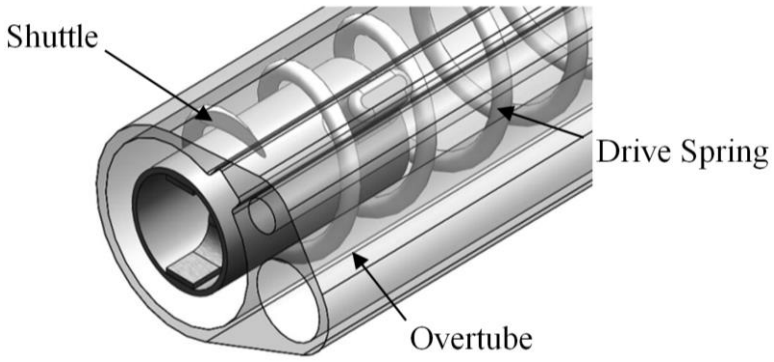

Figure 3-2 Material Handling System Cross Section [3-2]

While these materials are en route through the overtube they need to be secured so they do not come out of the shuttle and get stuck inside the overtube. Due to the small space inside the shuttle (⌀ 9.14 x 20.32 mm) the method of securing the payload needed to be simple and have a low part count to occupy the least amount of shuttle volume. A method of using compliant members to secure the payload was proposed because they could deform to accommodate the payload while securing it similar to a leaf spring. Since the shuttle would be interfacing with the *in vivo* robots the level of force necessary to

insert or remove the payload into the shuttle needs to be low, an amount achievable by the robots.

3.2 Retainer Design

Thin Nitinol ribbon was chosen as the retainer material to take advantage of its superelasticity since large deformations of the retainer would be necessary to accommodate large payloads that would occupy a majority of the shuttle. The retainer needed to have low lateral stiffness meaning that the force that would be required to remove an object out of the shuttle needed to be a level obtainable by the *in vivo* robots. Experimental tests have shown that the *in vivo* robots are capable of producing about 1 N of drawbar force [3-5] so consequently this level was used as a benchmark for how much force should be required to remove a payload from the retainer.

Samples of Nitinol ribbon were obtained from Memry Corporation (Bethel, CT) with widths of 3 mm and varying thicknesses of 0.2, 0.5, and 0.7 mm. It was determined by manual bending tests that 0.5 and 0.7 mm thick ribbon would not be able to deflect enough for payload insertion. A two piece retainer was used since it would centrally locate the payload and reduce the amount of deflection needed to accommodate the payload, as opposed to if a single ribbon spanned the inner diameter of the shuttle. One end of the ribbon would be fully fixed and the other free to allow for easier deformation when a payload is introduced (Figure 3-3).

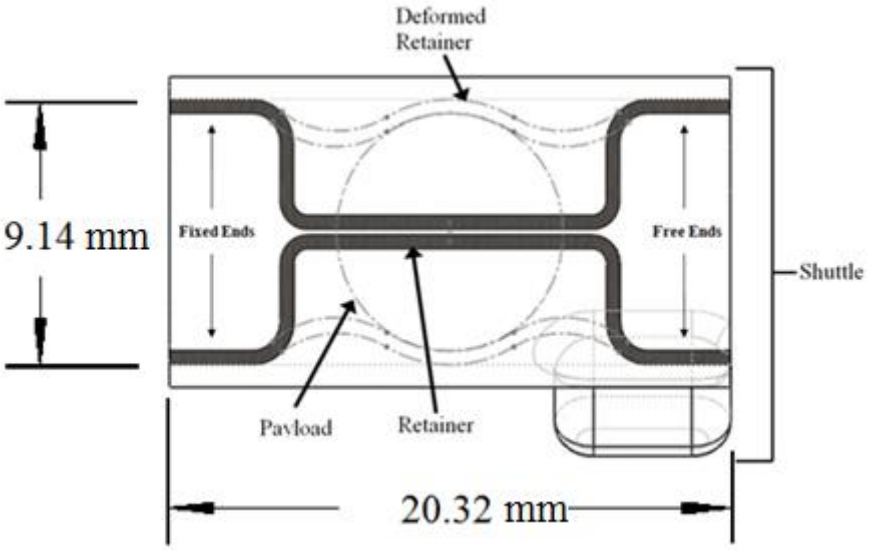

Figure 3-3 Schematic of Retainer Subassembly in the Shuttle

3.2.1 FE Analysis of Retainer Profile Shape

It was believed that the profile shape of the retainer greatly affected the grasping behavior so numerical modeling was done to gain a general understanding of this link. The relationship between the profile shape and the insertion force required to introduce an object into the shuttle as well as the clamping force experienced by the object was explored. Three general shapes were considered for the retainer profile shape: a plateau, double-peak, and single-peak, as seen in Figure 3-4.

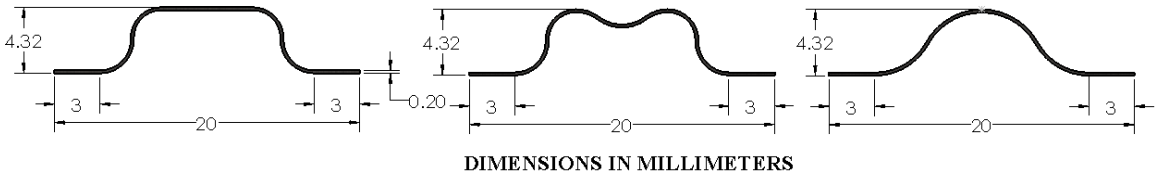

Figure 3-4 Ribbon Profile Shapes

3.2.1.1 Material Testing

Special consideration was given to the material properties of the Nitinol since it does not have a similar behavior to common engineering metals such as steel or

aluminum. Before modeling could take place, material testing needed to be performed to ensure the properties used in the simulation were accurate.

Uniaxial tensile tests were performed using an MTS 810 material testing system with a 25 kN load cell (Figure 3-5). Once the system was calibrated 50.8 x 3.0 x 0.5 mm samples were loaded into the grips and pulled to 8% strain, relaxed to 0 %, pulled to 8%, relaxed to 0%, then pulled to failure (Figure 3-6). This loading pattern was used because it would fully capture the hysteresis loop by unloading and unloading the samples before pulling them to failure. The samples were strained to 8% in accordance with the manufacturer's stated maximum recoverable strain. Before samples were loaded into the MTS machine they were heat treated in a furnace at 600°C for 10 minutes then water quenched. This was done to ensure simulation accuracy by putting the samples through the same heat treatment process that would later be used to shape set the Nitinol to the desired profile shape.

Figure 3-5 MTS 810 Material Testing System

Samples were pulled and relaxed at a strain rate of 0.001 (mm/mm)/s. Three samples were pulled and the average of their curves was taken for the single element study (Figure 3-7).

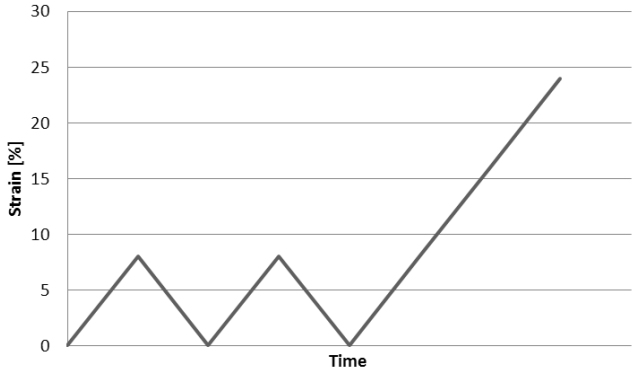

Figure 3-6 Tensile Test Load Curve

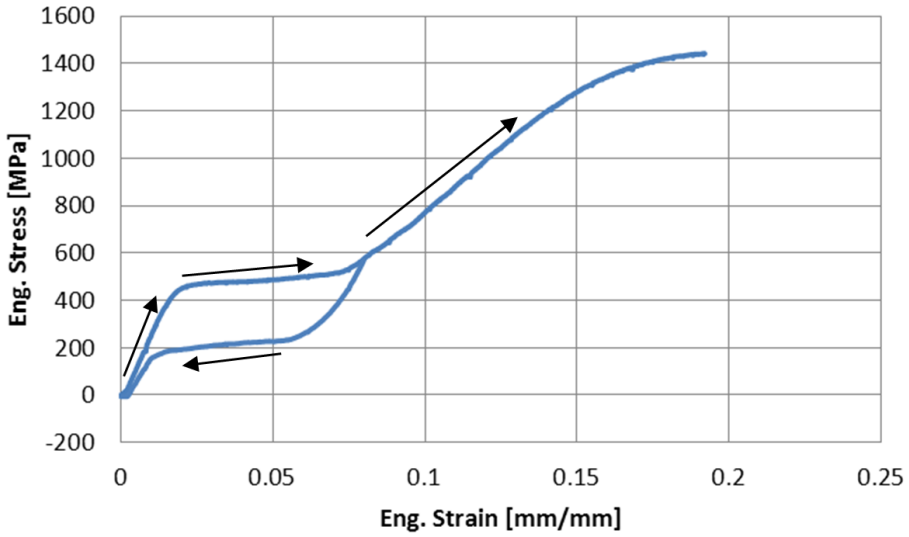

Figure 3-7 Average Nitinol Engineering Stress vs. Strain Curve

Values required for the material model included Young's modulus, density, Poisson's ratio, a parameter measuring the difference between material responses in tension and compression (α), Young's modulus for the martensite (YMRT), and the parameters shown in Figure 3-8. The density and Poisson's ratio were obtained from the manufacturer, and the default values for α and YMRT were used. To find the approximate value of the Young's modulus the linear section of the loading phase was isolated and a linear curve was fitted giving a Young's modulus of 24,862 MPa. The

transformation parameters and recoverable strain values were approximated by reading from the stress-strain curve in Figure 3-7 and given in Table 3-1.

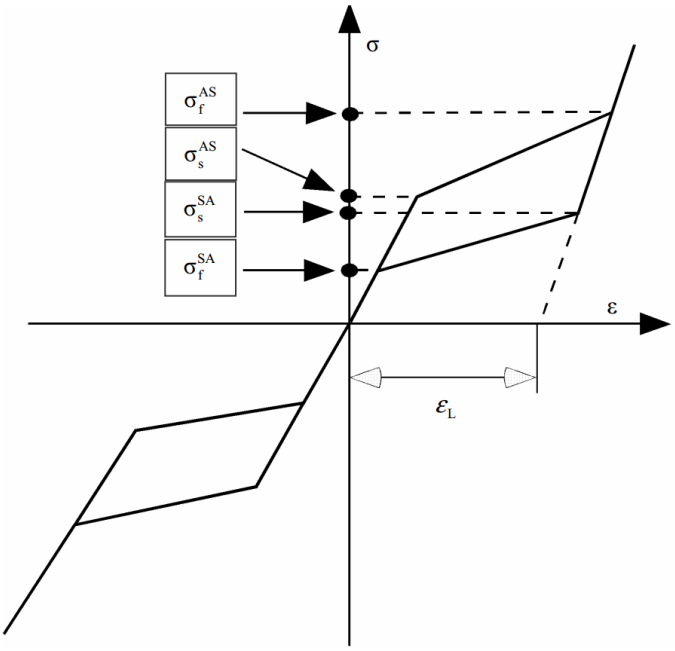

Figure 3-8 Required Parameters for Nitinol Material Model [3-6]

Table 3-1 Initial Nitinol Material Parameters

Parameter	Symbol	Value	Units
Density	ρ	6.45×10^{-3}	g/mm^3
Poisson's Ratio	ν	0.3	-
Young's Modulus	E	24862	MPa
Recoverable Strain	ε_L	0.0256	mm/mm
Starting value for forward phase transformation	σ_s^{as}	420	MPa
Final value for forward phase transformation	σ_f^{as}	543	MPa
Starting value for reverse phase transformation	σ_s^{sa}	251	MPa
Final value for reverse phase transformation	σ_f^{as}	110	MPa

3.2.1.2 Material Model

A single element study was performed to determine the correct material properties to be used in the FE analysis. A single shell element was loaded uniaxially in the same manner as the physical test using the shape memory material model and Belytschko-Tsay

shell element formulation. The results of the initial simulated pull test were plotted with the physical test data from the MTS machine and can be seen in Figure 3-9.

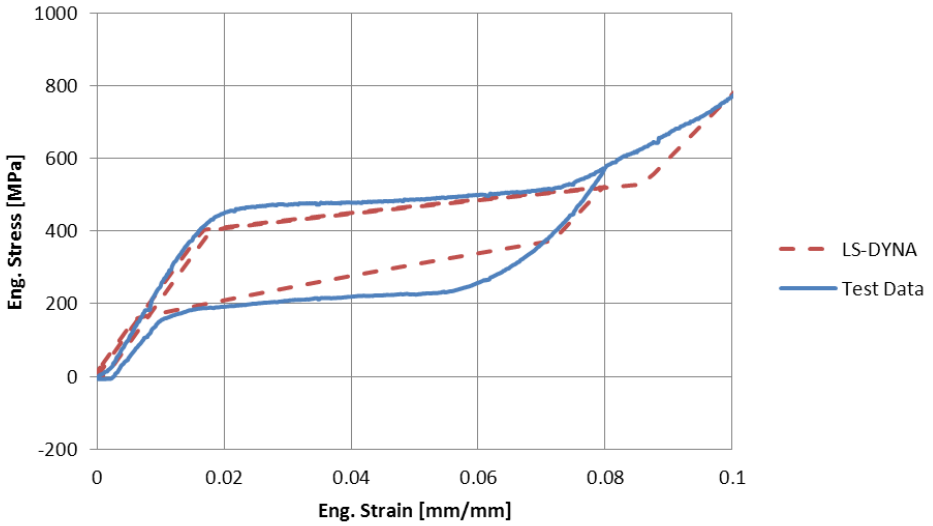

Figure 3-9 Initial Material Model Fitting

The initial estimation provided a close match to the test data but could be improved by adjusting the material parameters. By finessing the parameters a better match was obtained as seen in Figure 3-10 where the simulation results capture the hysteresis loop almost entirely. Table 3-2 gives the final values of the material parameters. The simulation model matches well with the test data up to about 8% strain but there is deviation at higher strain values. This deviation was ignored in the mean time since the strain was not expected to exceed 8% but this assumption was monitored in case a revision was needed.

Table 3-2 Final Nitinol Material Parameters

Parameter	Symbol	Value	Units
Density	ρ	6.45×10^{-3}	g/mm^3
Poisson's Ratio	ν	0.3	-
Young's Modulus	E	24862	MPa
Recoverable Strain	ε_L	0.052	mm/mm
Starting value for forward phase transformation	σ_s^{as}	440	MPa
Final value for forward phase transformation	σ_f^{as}	574	MPa

Starting value for reverse phase transformation	σ_s^{sa}	280	MPa
Final value for reverse phase transformation	σ_f^{sa}	161	MPa

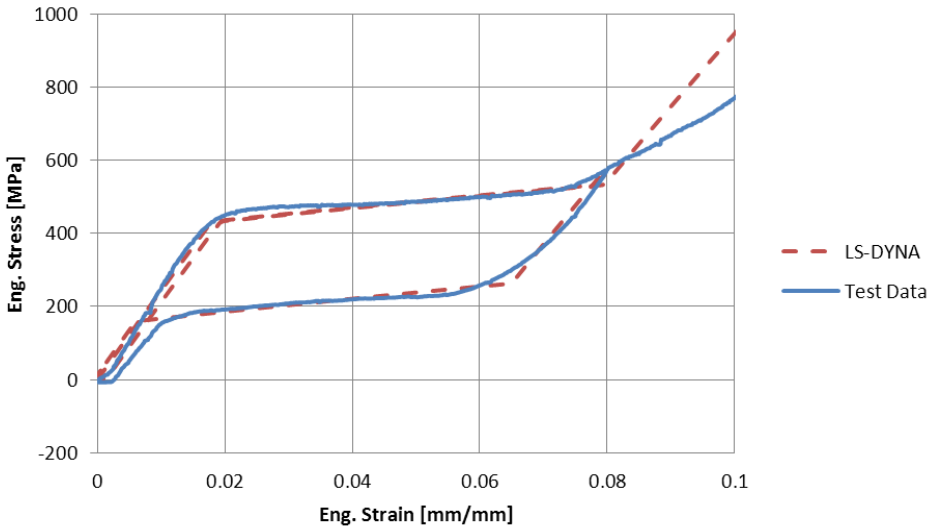

Figure 3-10 Final Material Model Fitting

3.2.1.3 Finite Element Simulation

The objective of the FE analysis was to determine how general changes in retainer profile shape affected the grasping behavior in terms of clamping and insertion forces. The three proposed shapes shown in Figure 3-4 were oriented in the same manner as they would be in the shuttle as seen in Figure 3-11. The shuttle was not included in the simulation but was replaced with stationary, planar rigid walls directly above and below the retainers.

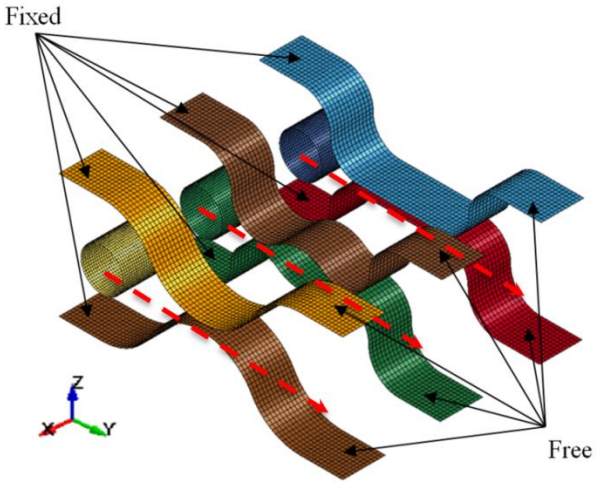

Figure 3-11 FE Analysis Setup

In this model all six retainers had their back ends fixed with the front ends left unconstrained to reflect their physical boundary conditions. A circular "pin" with 3 mm O.D., 3 mm in length, and 0.5 mm wall thickness was passed through the retainer from the fixed end to the free end on its transverse axis by applying a prescribed motion boundary condition to all the nodes in the pin. Each pin was positioned at the middle of each retainer pair to deform each top and bottom retainer equally as seen in Figure 3-12. Because the retainer had a shell thickness of 0.2 mm a contact thickness of 0.5 mm was used to prevent nodal release during contact. The automatic single surface contact algorithm was used throughout the model and force transducers were used between the pins and the two respective retainers they made contact with. The pins were constrained to allow motion only in the y and z directions in addition to no rotation. Motion in the z-direction was allowed to correct for any small errors in the vertical placement of the pins.

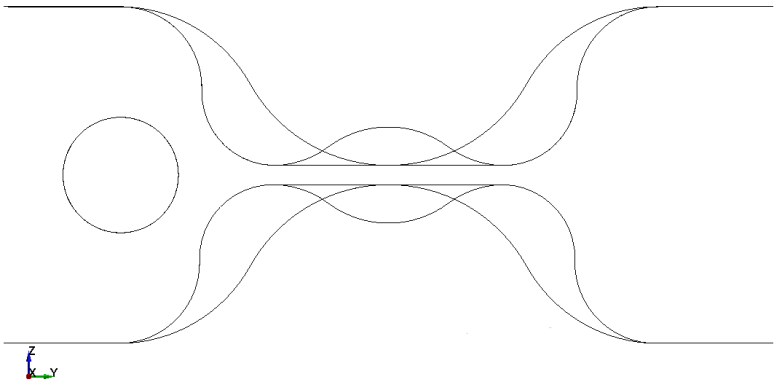

Figure 3-12 Pin Positioning

The retainers were meshed with Belytschko-Tsay shell elements with four integration points through the cross section. An element size of 0.25 x 0.25 mm was used in all retainer parts. The pins were also meshed with Belytschko-Tsay shell elements with four integration points through the cross section with an element size of 0.15 x 0.15 mm. An elastic-only material model was used for the pins with the properties of stainless steel.

3.2.1.4 Results

The simulation used 32 processors and executed in just under four and a half hours. Initial simulation runs demonstrated a need for hourglass control and element warping stiffness to combat instabilities in the model. Once a stable run was completed the resulting model was visually inspected to verify there were no remaining signs of instabilities such as element warping or hourglass modes in the elements. Figure 3-13 shows the progression of the pin through the retainer and the results are as expected. The assumption that the strain did not exceed 8% was verified by checking the maximum stress in the retainer. If the strain exceeded 8% then the stress would exceed the σ_f^{as} value of 574 MPa as a result. Fringe plotting the von Mises stress in the retainer shows a maximum value of 415 MPa, well below the maximum allowable value.

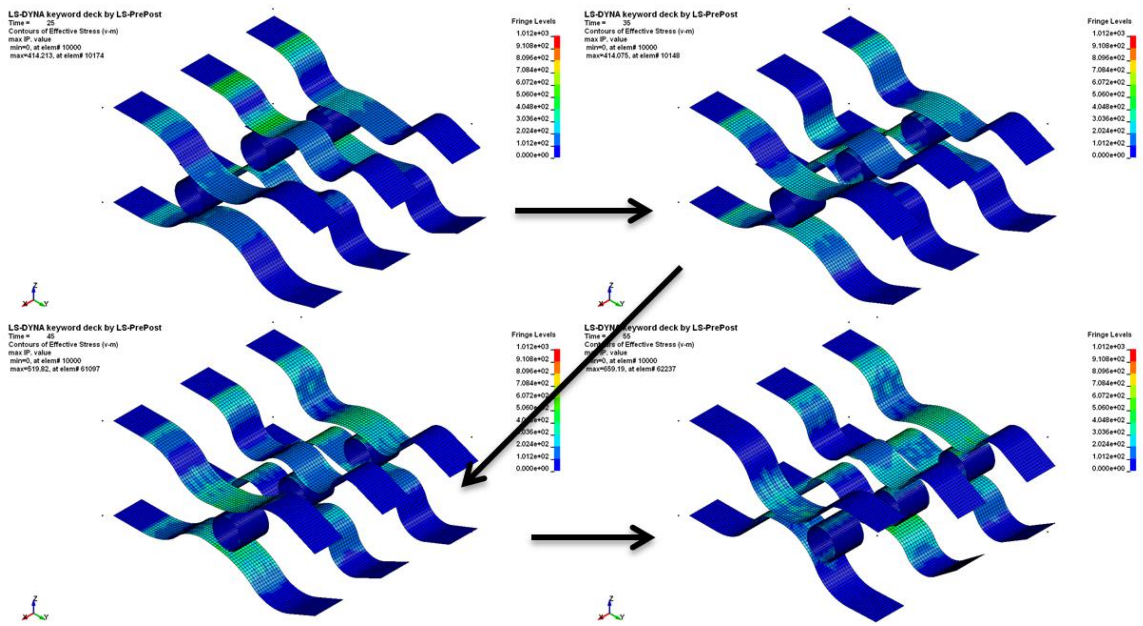

Figure 3-13 Progression of Simulation

The main objective of this study was to examine the differences in grasping behavior between the three profile shapes. This was quantified by the insertion force, the contact force between the pin and retainer in the y-direction, and the clamping force, contact force in the z-direction as seen in Figure 3-14.

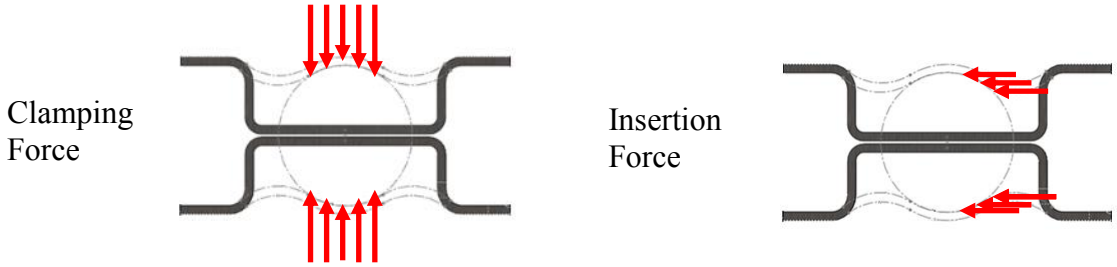

Figure 3-14 Clamping and Insertion Forces

These two forces are calculated in the simulation by implementing the force transducer feature in LS-DYNA. For this simulation, force transducers measure the clamping and insertion forces between two parts (i.e. pin and retainer) by summing the contact forces along all segments of the parts in contact. So the clamping force is calculated by

summing the z-components of the contact force vector between two parts and the insertion force is calculated by summing the y-components of the contact force vector. For reference, Figure 3-15 shows the division of the different profiles into sections with transition points referring to the locations where the red lines cross the retainer.

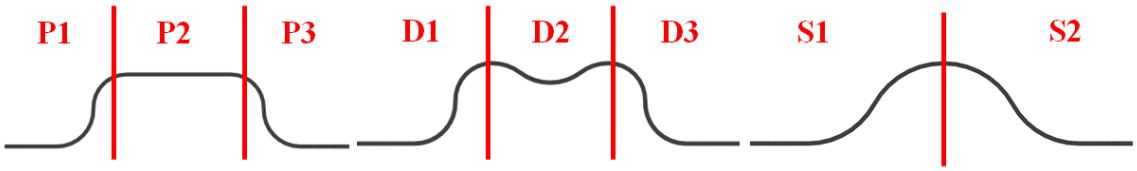

Figure 3-15 Retainer Sections

Examining the clamping force shows some clear differences between the profile shapes (Figure 3-16). As the pin passes through the retainer both the plateau and double-peak profiles increase in clamp force to their maximum value at the transition point between sections 1 and 2. The clamp force then decreases to a local minimum as the pin reaches the middle sections (P2 & D2). As the pin passes into the final section there is a last increase in clamp force before the pin exits the retainer. The decrease in section D2 is more pronounced than in P2 because of the differences in shape between the two profiles. The physical dip in section D2 creates a small pocket for the pin (Figure 3-15), reducing the deformation of the retainer. The single-peak profile shows a gradual increase in clamp force as the pin passes through the retainer and upon crossing over into section S2 the clamping force decreases with no local minimum.

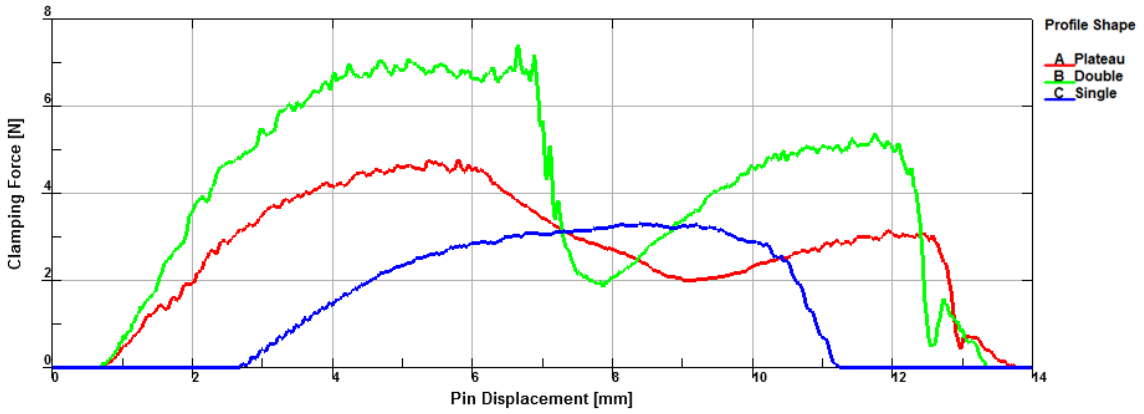

Figure 3-16 Clamping Force

Comparing the insertion forces of each profile shape reveals some interesting behavior. As the pin passes through the retainer the insertion force initially acts in the negative y-direction, opposing the motion of the pin. It reaches a maximum negative value at about 2.5 mm (Figure 3-17) into the retainer before increasing and becoming positive around 5 mm. At this point the pin is being grasped unstably because any deviation from this point of zero insertion force pushes the pin away from its current position, whether it is positive or negative displacement. Moving the pin in the negative direction from this point creates a negative insertion force that will move the pin back towards the fixed end where it was inserted. Conversely moving the pin in the positive direction creates a positive insertion force that will move the pin forwards towards the free end of the retainer. This unstable grasping is graphically represented by a point of zero insertion force where the derivative of the insertion force with respect to the pin displacement is positive. The pin then experiences stable grasping around the 8 mm mark for both the plateau and double-peak profiles. At this point the insertion force is zero but the derivative of the insertion force is negative. This means that any displacements of the pin from this point of zero insertion force will result in an opposing insertion force that

resists pin motion, hence stable grasping. The magnitude of the derivative also tells how stable or unstable grasping is. Highly stable grasping is evident by negative derivatives large in magnitude, and highly unstable grasping is evident by positive derivatives also large in magnitude. Stable and unstable grasping are also correlated to the geometric features of the retainer. Unstable grasping occurred when the pin was clamped in the retainer by convex features such as the transition points between sections 1 and 2 as well as sections 2 and 3 in both the plateau and double-peak shapes. Stable grasping occurred when the pin was clamped by concave sections of the retainer. The single-peak profile only exhibits unstable grasping behavior and for that reason would not make a good retainer for this NOTES application. The plateau shaped profile would be the best option because it has a stable grasping condition and the magnitudes of its insertion forces are lower than the double-peak profile which would benefit both the surgeon inserting a payload into the shuttle and the *in* vivo robots extracting the payload while still clamping the payload sufficiently. For this situation, using the plateau shaped retainer, the robot would need to generate about 2 N of force to pull a 3 mm “pin” out of the shuttle which may be slightly more than what the robot is currently capable of producing (approximately 1 N).

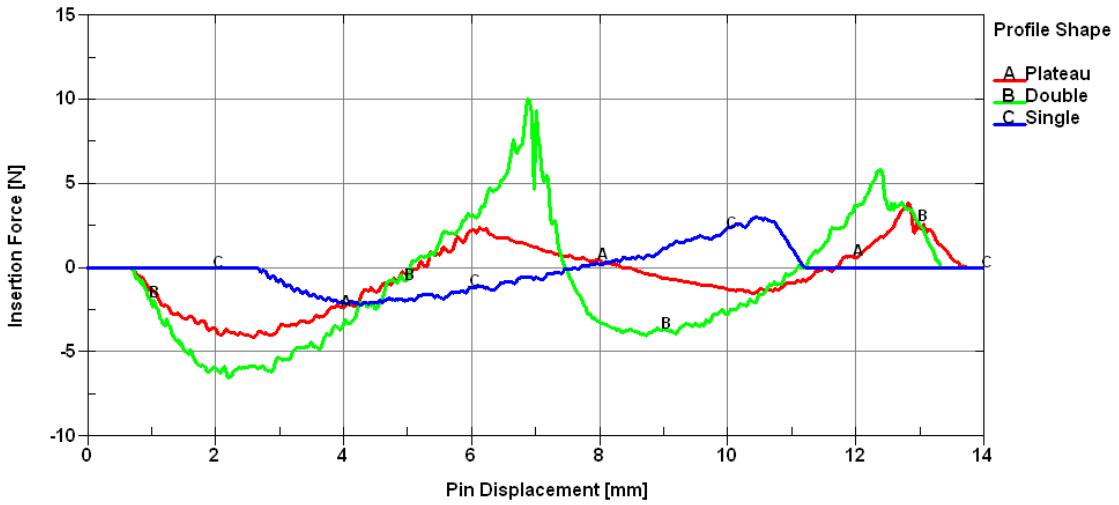

Figure 3-17 Insertion Force

3.3 Fabrication

To form the Nitinol retainer to the desired shape it needed to be heat treated in a fixture. Before heat treatment the Nitinol strip would be straight, as-rolled in ambient conditions. After the constrained heat treatment the strip would remain in the shaped form upon cooling. A simple fixture was made (Figure 3-18) for the retainer consisting of a 0.25” thick steel plate with six 4 mm steel pins press-fit into the plate.

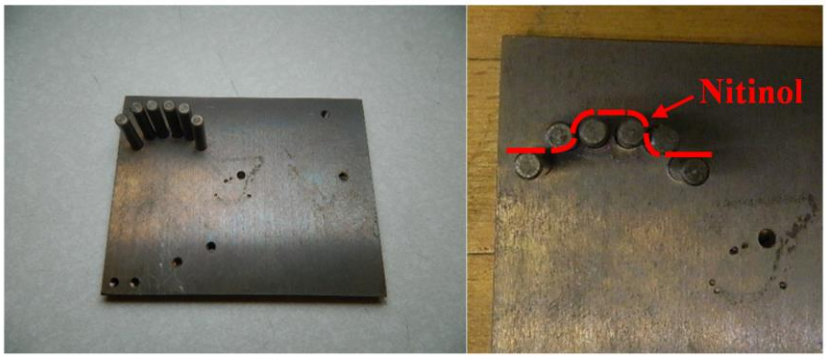

Figure 3-18 Heat Treatment Fixture

The Nitinol strip was threaded around the pins and pulled tightly on the ends with pliers to achieve the shape shown in Figure 3-18. The fixture was then placed in an oven

and heat treated at 600°C for 10 minutes, then immediately water-quenched. This process was repeated for the second strip of Nitinol. Upon examination of the Nitinol after it had cooled it was observed that the upper surface of the plateau was not flat but rounded. This occurred because despite pulling on the retainer with pliers there was still slack in the Nitinol as it bent over the top two pins. As a result the plateau height was too tall which would cause the retainers to be preloaded once they would be put in the shuttle. To remedy this, the Nitinol was heat treated again between two steel plates spaced 4.3 mm apart with 2 pieces of 0.5 x 0.26" aluminum tube cut to 4.3 mm in length. This second stage heat treatment reduced the height of the plateau and did not change the overall shape of the retainers. The retainers were then glued into the shuttle using J-B KwikWeld at one end of the retainers while leaving the other end free as illustrated in Figure 3-3.

3.4 Physical Testing

Benchtop testing was performed to examine performance of the retainer before testing in a porcine model. Surgical staples and a robotic end effector were separately inserted into the shuttle and the shuttle was shaken vigorously. The tools did not come out of the shuttle and were held securely. It was observed that the free ends of the retainer extended beyond the footprint of the shuttle approximately 2 mm while the end effector was inserted. This will need to be monitored when cooperative testing is performed with any *in vivo* robots because the extension of the retainer may interfere with the robots removal or insertion of objects into the shuttle. This qualitative evaluation was determined to be a sufficient measurement of performance and the retainer along with the rest of the material handling system was deemed ready for animal testing.

In vivo testing on a non-survivable porcine model was performed. The objective of this test was to insert the Material Handling System transvaginally and introduce it into an insufflated abdominal cavity and verify the functionality of the device in the harsh environment. Details of the procedure can be found in a previous thesis [3-2]. The MHS was able to navigate to the abdominal cavity and transport the shuttle through the overtube as seen in Figure 3-19.

Figure 3-19 Fully Inserted Shuttle, Dyed Blue For Visualization [3-2]

A surgical staple was loaded into the shuttle by the surgeon and transported to the distal end of the overtube inside the abdominal cavity. The staple remained securely grasped in the shuttle and was removed inside the abdominal cavity with a laparoscopic grasper, reinserted into the shuttle, and transported to the opposite end of the MHS. This test provided a feasibility model by demonstrating the retainer could hold onto the payload inside the shuttle during a procedure and not be affected by the harsh environment of the abdominal cavity.

Chapter 4 Compliant Laparoscopic Grasper

4.1 Motivation

In laparoscopic surgery, long shafted tools are inserted through small incisions in the patient to access the surgery site with the ultimate goal of reducing trauma to the patient and decreasing recovery time. Since surgeons are using these tools to manipulate tissue during the procedure there is a loss of tactile feedback [4-1]. With this loss, a surgeon may either apply excessive or insufficient forces to tissues during manipulation. In the case of insufficient force, tissues would slip out of the grasper and surgery time would increase as a result of the repeated actions. When excessive force is applied, inadvertent consequences can arise such as tissue perforations and trauma [4-2], putting the patient at risk. As an example, bile and gallstone spillage has been reported as a complication in laparoscopic cholecystectomy as a result of perforations in the gallbladder from the teeth of the grasper instrument [4-3]. If the spilled stones were not completely removed, reported post-operative complications included both abscess and fistula formation [4-3], bowel obstruction [4-4], and bowel perforation [4-5]. In some cases open surgical procedures were needed to remedy these complications.

Efforts have been made to lessen this risk by either modifying or redesigning graspers. Adding a curved edge to the jaw tip and fitting the jaw with a compliant tip has been shown to reduce the maximum pinch forces [4-6,7] but these two approaches do not address the distribution of the pressure generated by the jaws which is concentrated at the jaw tip [4-8]. Other examples include integrating electronic hardware with the grasper in a master/slave or embedded configuration [4-9] with the goal of regaining force

feedback. However these technologies are still dominated by basic level research and have yet to produce opportunities for standard clinical use [4-9].

What is proposed here is to replace the rigid metal jaw that is commonly found in commercial graspers with a fully compliant, monolithic jaw that deforms as it grasps tissue. It is hypothesized that grasping soft tissue in a more compliant manner will reduce the maximum pinch forces seen by the tissues. This way a surgeon can grab and manipulate tissue without worrying if unnecessary trauma is being caused.

4.2 Jaw Profile Design

The design objective was to achieve a compliant jaw profile that opens and closes through the central linear actuation of a push/pull rod in a laparoscopic tool, without generating the tissue stress concentrations seen in rigid tool designs [4-6,7]. It has been recommended that safe laparoscopic graspers should be able to transmit at least 5 N of pull force to the soft tissue without damaging it [4-10] and this recommendation was used as a benchmark. By replacing rigid links and kinematic joints with compliant members, it is possible to utilize the unique compliance characteristics to transfer the push/pull actuation into opening and closing jaw motion. This also introduces other advantages such as lower part count and reduced friction effects. The approach taken was to have the outside of the jaw (1) fixed to a stationary outer tube (3) that encases the push/pull rod (2) as seen in Figure 4-1. In this general configuration the outward displacement of the rod (red) will deform the jaws in a manner that will result in the jaws opening (red). Conversely the inward displacement of the rod (green) will result in the jaws closing.

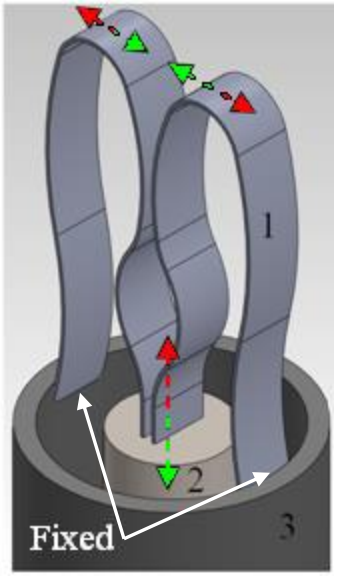

Figure 4-1 3D Concept Grasper Showing Opening (Red) and Closing (Green) Motions

Fourteen different jaw profiles were modeled and analyzed in ABAQUS using the material properties from the previous chapter to evaluate the motion achieved by linear displacement of the inner leg of the jaw. In the simulation, the outside legs were fixed in all directions and a one degree of freedom displacement boundary conditions was applied to the inner legs to mirror the physical actuation from the central rod (Figure 4-2). The jaws were first opened then fully closed to capture the full intended range of motion.

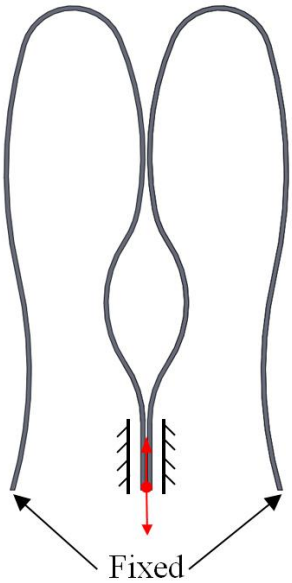

Figure 4-2 Boundary Conditions for Grasper Simulation

By examining the differences in the opening and closing behavior from changes in the profile shape, revisions were made to the jaw profile until a reasonable shape was reached. It was desired that the jaws made contact in a way that the generated pinch force was distributed on a surface instead of concentrated at a point; therefore reducing the trauma experienced by the tissue. It was also required that the jaws do not contract, or shorten in length, when they close as a result of the ribbon bending. The initial jaw shape (Rev1), shown in Figure 4-3, was very crude and basic. Through iterations it was learned that curving the straight segments resulted in less collapsing of the jaws and more rotational opening and closing motion. It was also learned that if the Nitinol was to be pulled by the central push/pull rod the inner legs of both jaws needed to be placed side-by-side instead of having a gap between them as earlier revisions did. If there was a gap between the inner legs the jaws would not come together in the fully closed state, leaving a space between the jaws where tissue would not be grasped.

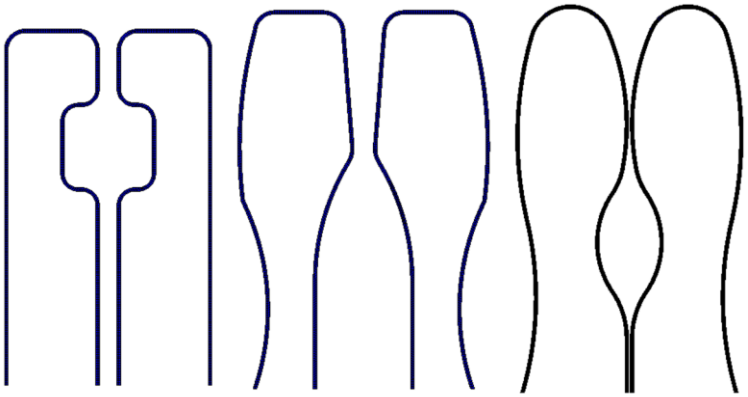

Figure 4-3 Jaw Profile Shapes: Rev1, Rev5, Rev13

A progression of profile shapes and their revisions can be seen in Appendix A. The final shape, shown in Figure 4-4 with dimensioned drawing in Appendix B, was designed so that the default state of the jaw was open instead of closed. This change was made because a closed default state would require double-action actuation meaning the push rod would have to advance out of the outer tube to open the jaws then retract to close jaws. Having an open default state requires only single-action actuation where only rod retraction is needed to close the jaws. This translates to the user only having to squeeze the trigger to close the jaws instead of opening then squeezing the trigger.

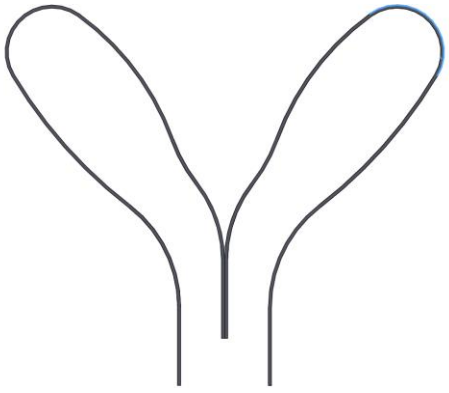

Figure 4-4 Final Open Jaw Profile Shape

4.3 Jaw Fabrication

To fabricate the jaw a compression die (Figure 4-5) was cut out of mild steel using wire EDM (electrical discharge machining) for the heat treatment of the Nitinol. This method of constraining the Nitinol was used instead of the previous pin-in-plate jig for two reasons. First, the shape of the jaw is more complex than the retainer shape described in the previous chapter, and second, using the jig did not give the best results. The features of the retainer did not come out exactly as desired which meant a secondary heat treatment needed to be performed. Using a compression die gave a better control over the shape of the Nitinol and no secondary processes were needed. The heat treatment schedule on the other hand was the same. Two 55 mm Nitinol ribbons were placed into the die and heat treated for 10 minutes at 600°C and then immediately water quenched.

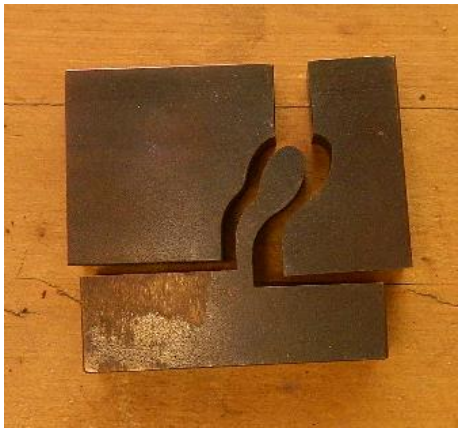

Figure 4-5 Compression Die for Heat Treating the Nitinol (screws not shown)

4.4 Grasper Handle Design

A simple grasper was fabricated for testing purposes (Figure 4-6) since the jaws were the area of focus. Extra features that may be found in commercial graspers were not included, such as rotating jaws and a ratcheting handle. The ⌀ 3/16” push/pull rod (black) is constrained to prismatic translation by the pin (red) at the top of the trigger through a

fixed front panel (fuchsia) in the handle casing and a thin ⌀7/32” aluminum tube (orange). The handle casing and trigger were laser cut from ¼” acrylic and glued together with a 2-part epoxy. Actuation of the jaws was simplified such that squeezing the trigger would laterally translate a push/pull rod through a pin-slot configuration at the top of the trigger, with the trigger pivoting at its base near the bottom of the handle as seen in Figure 4-7.

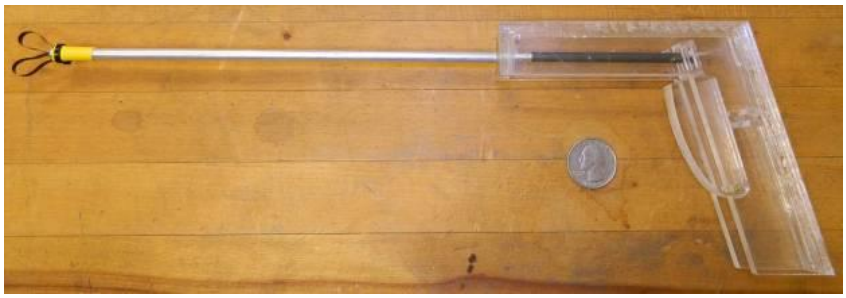

Figure 4-6 Simple Grasper for Testing

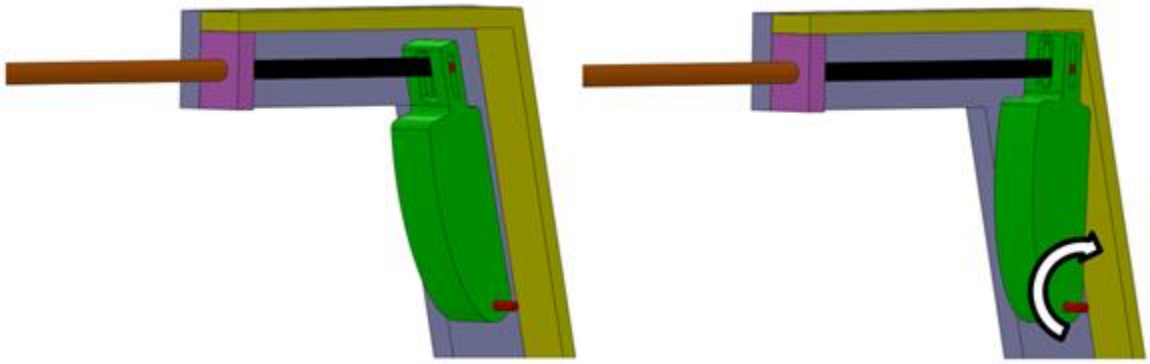

Figure 4-7 Rotated Trigger View in CAD (Front Cover Hidden)

This lateral motion directly opens and closes the jaws by either pushing or pulling the inner legs of the jaw, causing the jaws to open or close respectively as seen in Figure 4-8. The push rod is attached to the jaw inner legs while the outer legs are fixed to the aluminum outer tube. It was desired to have a nonpermanent method of fixing the jaw to the outer tube during the development and testing stages; this was achieved by using a

zip-tie and heat-shrink tubing to temporarily fix the outer jaws. The jaws have a natural spring-back behavior due to the stored energy from deflection, so the jaws open by themselves when the trigger is released.

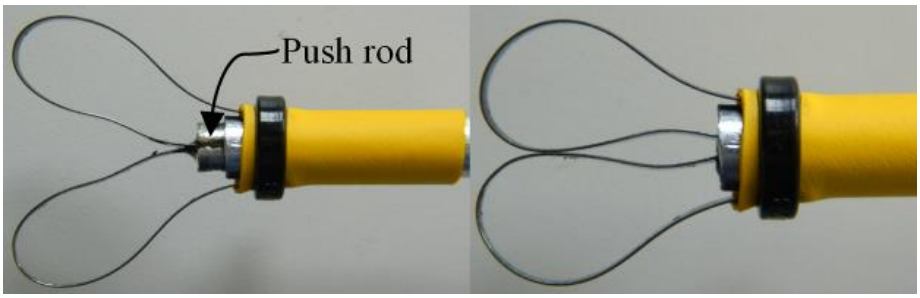

Figure 4-8 Jaws Shown Open and Closed

4.5 Testing

Two tests were performed to quantitatively assess the grasper's capabilities. The first was to quantify the pinch force the compliant jaws were capable of producing whereas the second test was designed to determine the maximum pull force the jaws could exert on tissue before losing traction. The tests were performed with the prototype compliant grasper and a commercially available rigid grasper (AutoSuture™ Endo Clinch™ II 5mm, Mansfield, MA) for comparison.

4.5.1 Pinch Force

An A201 FlexiForce® sensor (Tekscan Inc., South Boston, MA), a thin-film force sensitive resistor (FSR), was used to record pinch force data during testing. The graspers and resistor were fixed spatially (Figure 4-9) so the jaws could clamp the sensor in the same location within the sensor's active area to ensure repeatability. A piece of scrap ¼" acrylic was fastened to a 2" thick piece of wood with screws and the grasper was attached on top of the acrylic with double-sided tape. Again using double-sided tape, the FSR was attached to a piece of 1/8" acrylic which was fixed to the wood with three screws as seen

in Figure 4-9 to prevent vertical motion. The FSR was attached so that the active area hung over the edge of the acrylic so it could be pinched from both sides. Lateral motion was allowed to adjust the sensor position just prior to testing so the jaws interacted with the active area.

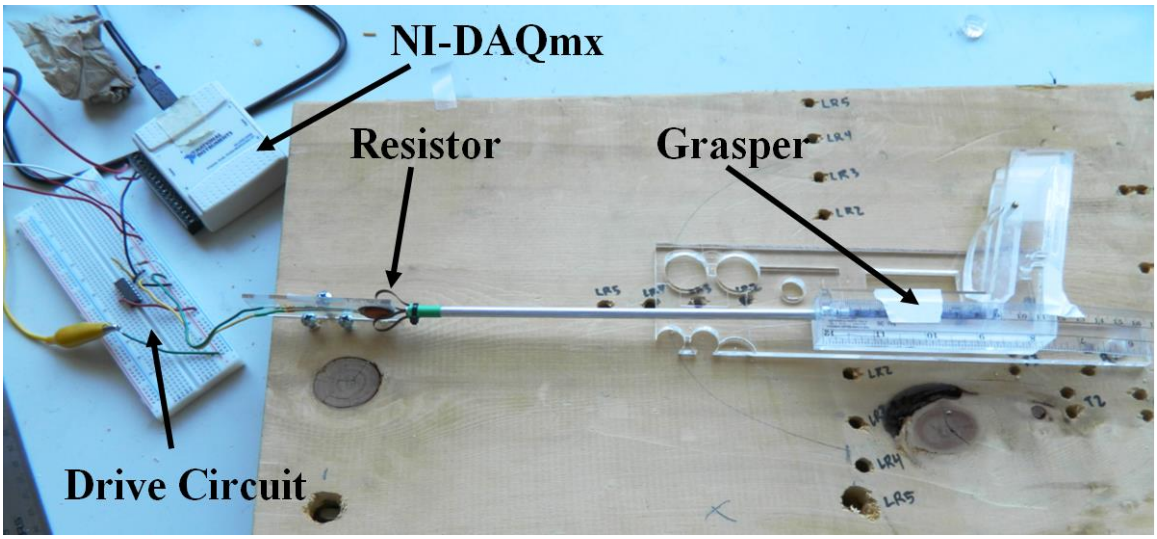

Figure 4-9 Pinch Force Test Fixture

4.5.1.1 Drive Circuit and Calibration

A drive circuit with a +6V input was used based on a manufacturer's recommendation to convert the pinch force seen by the sensor into an analog voltage signal. The drive circuit (Figure 4-10) uses a voltage divider with a measuring resistor (RM) to control the force sensitivity range, and a current limiting LM324 op-amp was used at the manufacturer's recommendation. This gives an output voltage equation of:

$$V_{out} = \frac{V_+}{1+\frac{R_{FSR}}{RM}} \quad (1)$$

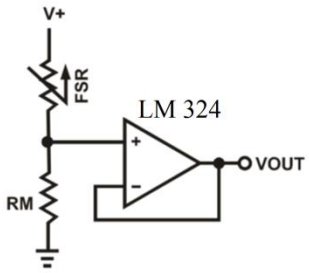

Figure 4-10 FSR Drive Circuit [4-11]

Once the circuit was set up, it needed to be calibrated to derive a relationship between the force applied to the FSR and output voltage of the drive circuit. Brass weights were incrementally placed on top of the sensor and the output voltage was recorded. Since the diameter of the brass weights were larger than the active area on the sensor, two disks were cut from 0.023" steel shim stock and taped to the front and back of the FSR using double-sided tape. This assured that all the force from the weights was seen by the FSR. These values were plotted and a linear relationship was developed as seen in Figure 4-11.

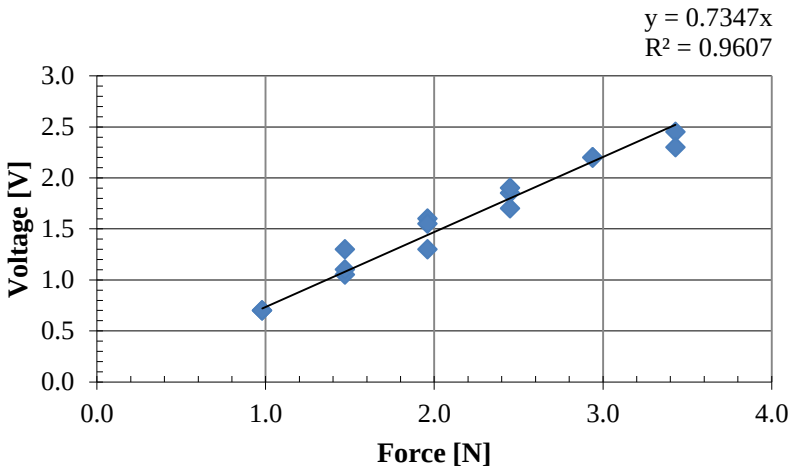

Figure 4-11 FSR Calibration

To get the necessary sensitivity and range, the measuring resistor (RM) needed to be adjusted during calibration with a final resistor value of 680 kΩ used in the circuit. The

output voltage was read with an NI-DAQmx data acquisition device and displayed using a simple LabVIEW program (VI found in Appendix D).

Once the drive circuit was calibrated, the pinch force from the grasper was recorded. The trigger was pulled so that the central push rod displaced in discrete increments. This was accomplished by taping a transparent ruler on the handle casing so the position of the rod/trigger pivot pin could be read off the ruler as seen in Figure 4-12. A C-clamp was used to keep the trigger at the desired position while the output voltage from the drive circuit was read and recorded. The output voltage was allowed to settle to a relatively constant value before being recorded.

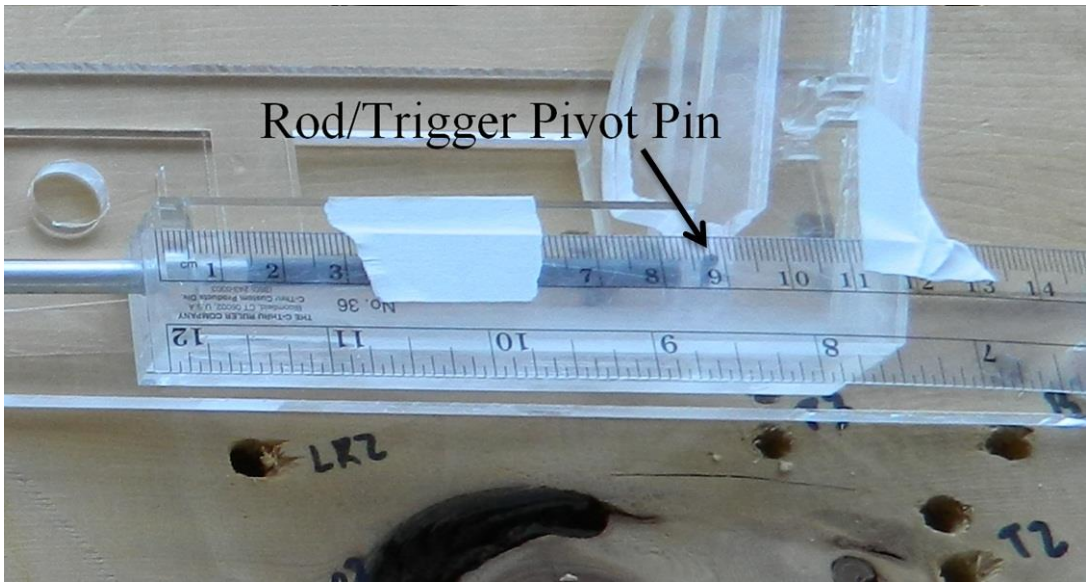

Figure 4-12 Measuring Rod Displacement

4.5.2 Pull Force

Tests were performed to determine the maximum pull force the graspers were capable of producing. Porcine liver samples 2x7x0.5 cm in size were clamped in the grasper on one end with the trigger fully squeezed (Figure 4-13). Weight was then added incrementally on the other end until the tissue slipped out of the jaws. Thirteen and nine

trials were done with the compliant and rigid graspers respectively, with new samples used for each trial. Each trial lasted approximately one minute and the tissue samples were kept wet during until they were used.

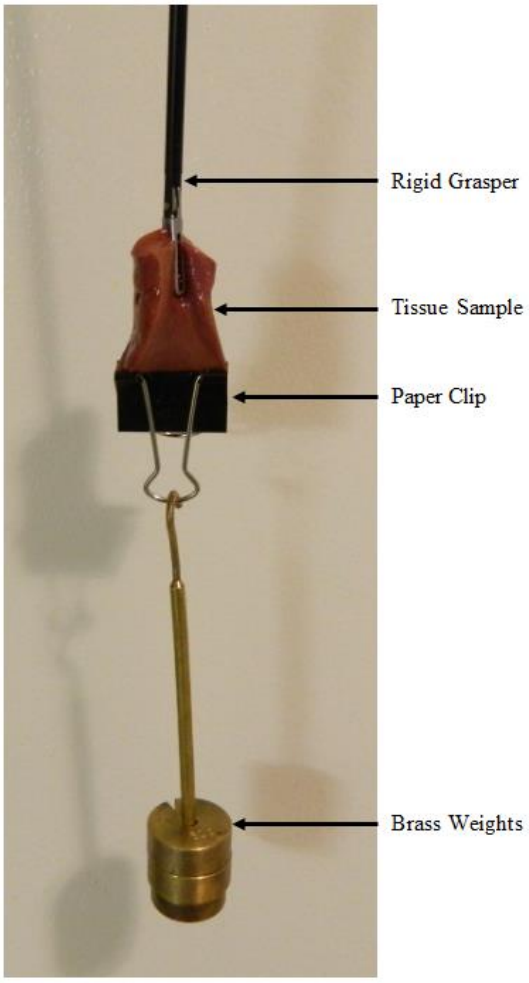

Figure 4-13 Pull Test Configuration

4.6 Results

4.6.1 Pinch Test

Pinch force data for the compliant grasper were recorded as a function of the linear displacement of the push rod. The trigger was squeezed to translate the rod in 1

mm increments. Figure 4-14 shows the relationship between the push rod displacement and the pinch force of the compliant grasper.

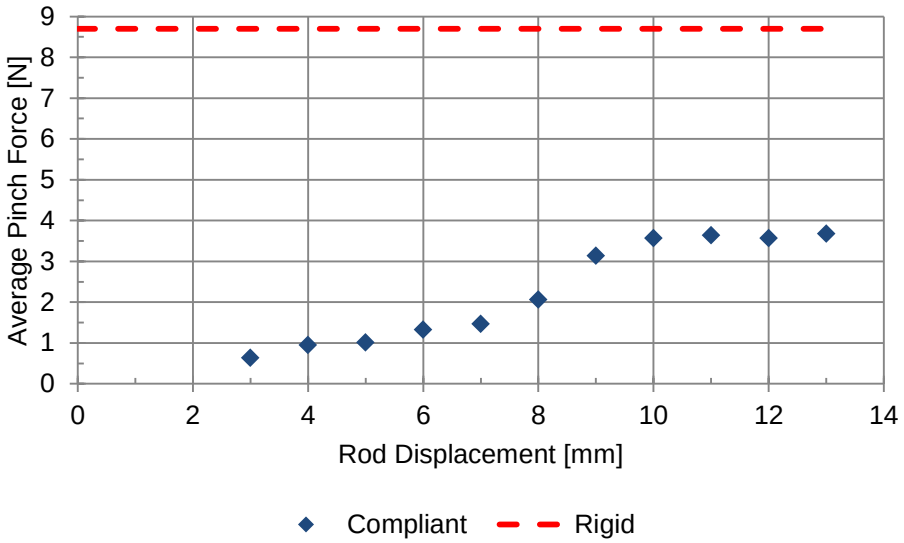

Figure 4-14 Compliant and Rigid Grasper Pinch Force

It was not possible to record the pinch force for the rigid grasper as a function of the displacement of its push rod since there was a considerable amount of play between the trigger, push rod and jaws due to the pin-in-slot joints at the jaws-and-rod and trigger-and-rod joints. The maximum pinch force of the rigid grasper was recorded over 10 trials with an average of 8.7N.

The pinch force data for the compliant grasper shows an interesting and possibly useful behavior. The relationship between the rod displacement and the pinch force is generally sigmoidal in shape, with the initial portion being fairly linear, a rise around the 9 mm mark, and a plateau around 3.5N at 10 mm. With the trigger fully squeezed, the jaws were pinched manually and the reading jumped simultaneously. This was done to verify that the sensor did not reach an upper limit and incorrect measurements were taken. The inherent maximum pinch force of the compliant grasper could prove to be

useful in mitigating tissue trauma. By having a “built-in” maximum pinch force a surgeon can fully squeeze the trigger and not worry about applying excess force that can damage the tissue.

It was observed during testing that in the linear region, the contact area between the grasper and FSR sensor was increasing as the jaws closed around the sensor, and at 9 mm of displacement the jaws were fully in contact with the sensor. During the later stages of closure the jaws also pulled the sensor towards the grasper as it pinched. This behavior was different than what was observed with the rigid grasper. Since the rigid jaws pivot at their base, the resulting grasping motion was a combination of pinching and pushing the sensor away from the grasper. This pinching/pushing behavior is counterintuitive to what would constitute efficient grasping since it moves the tissue in the opposite direction of the intended stretching.

4.6.2 Pull Force

The results for the pull tests are summarized in Table 4-1. For each trial both graspers were closed as tight as possible to achieve the maximum pull force. In the case of the rigid grasper which had 1 mm teeth, significant trauma was observed in the tissue samples following each trial as seen in Figure 4-15.

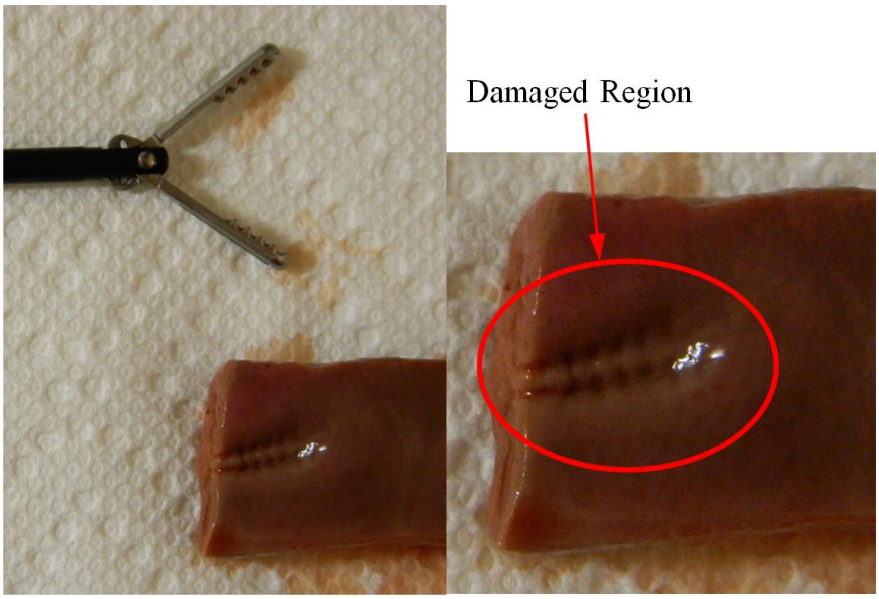

Figure 4-15 Example of Tissue Damage as a Result of Applying Excessive Pinch Force

Table 4-1 Pull Test Data

	Avg. Max. Pull Force [N]	Std. Dev. [N]
Compliant	1.4	0.6
Rigid	8.1	0.6

It was expected that the prototype compliant jaw would have an inferior maximum pull force compared to the rigid grasper since the interface between the jaws and tissue is toothless. It was found that laparoscopic graspers should be able to achieve at least 5N of pull force [4-10] without causing damage. It was observed that the compliant graspers caused minimal to no trauma to the tissue following each pull test trial, while significant damage (i.e., large perforations and torn tissue) was observed on samples grasped by the rigid graspers.

4.7 Increasing Traction

The traction between the jaws and tissue needed to be improved to make the compliant grasper useful in a surgical setting. One option was to add teeth features

similar to rigid grasper used for testing, but that would entail adding a small wave-like pattern to the jaw profile (Figure 4-16) that would not be physically obtainable using the heat treatment method due to the stiffness of the Nitinol. Another option would be to add a rough texture to the surface of the Nitinol through a secondary process such as knurling. This option was not pursued since the thickness of the Nitinol was only 0.2 mm and the integrity of the ribbon would be at risk.

Figure 4-16 Conceptual Wave Pattern for Jaw Teeth

Treads made of polydimethylsiloxane (PDMS) have been shown to improve traction and mobility in wheeled crawler-type *in vivo* robots for medical applications [4-13] with the use of circular micro-treads 140 μm in diameter, 70 μm tall, and spaced 105 μm apart (Figure 4-17) showing an increase in traction of 50 – 100% [4-12]. From this it was believed that applying PDMS treads to the jaws of the compliant grasper would improve the pull force it could apply to tissue without damaging the tissue.

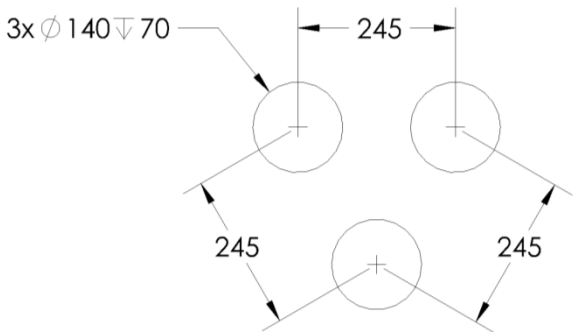

Figure 4-17 Tread Pattern From [4-13] (Units in μm)

To make the treads, a mold was needed to pour the liquid PDMS into for curing. In photolithography micro-molds are made on silicon wafers with a layer of photoresist serving as the mold negative. The process to fabricate this mold is quite intricate [4-14] and requires nanofabrication equipment which is not commonly available. As a result, a cheaper alternative was pursued that involved laser machining a mold negative into ¼" acrylic sheet using an Epilog Mini 18 laser system with a 30 Watt CO_2 laser. It was unknown how small of a hole this laser system could make so test cuts were made to determine what combination of cutting parameters, laser power and cutting head speed, produced the smallest and shallowest blind holes.

Using CorelDraw software, different hole sizes of 127, 102, 76, 51, 25, and 13 microns in diameter were drawn to determine if the laser system could make holes this small. Recommended speed, power, and frequency settings for cutting through ¼" thick acrylic were 5%, 100%, and 5000 Hz respectively [4-15]. The speed setting was increased to 30% since through holes were not wanted as they would serve no purpose in the mold. This speed setting proved to be too slow since the holes that were created came out very distorted and non-uniform when viewed under a microscope as seen in Figure 4-18.

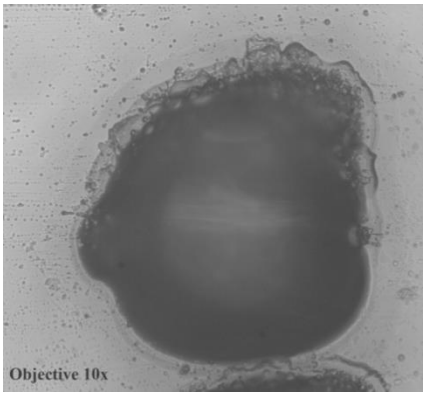

Figure 4-18 Magnification (10x) of Hole Cut at 30% Speed

The speed setting was increased incrementally and the holes were inspected until uniform holes were cut. Figure 4-19 shows the results from speed settings of 80%, 90%, and 100%. At 80% the holes are still distorted but starting to resemble a circle. There is also an overlap of the heat-affected zone (HAZ) of the base material between the holes, which is revealed by the many air bubbles in the acrylic. At 90% the holes are becoming less distorted and the HAZ is reduced. A speed setting of 100% produced the best results with the least amount of distortion and a very small HAZ that does not seem to overlap. At higher speeds the laser-cut holes became more uniform because the reduced exposure to the laser beam prevented the area surrounding the laser from melting. The 100% setting was selected because it produced the most uniform hole and had the smallest HAZ.

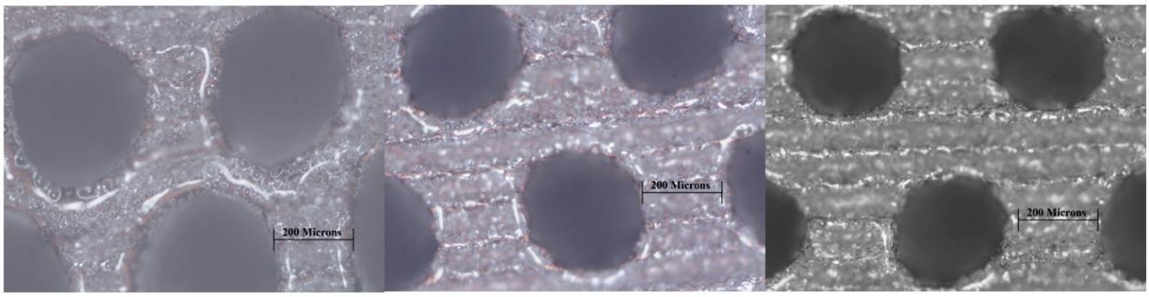

Figure 4-19 Hole Cut with 80%, 90%, and 100% Speed Setting (L-R)

In verifying the hole sizes it was found that the laser system could not achieve the small hole sizes that were desired. A 25 micron diameter hole drawn in CorelDraw ended up having an actual hole diameter of 254 microns which appeared to be the smallest possible hole size since a desired hole size of 51 microns ended up being 305 microns. Therefore it was not possible to make the pattern shown in Figure 4-17. As a result, the following pattern was used for the mold, which kept the 1.75 aspect ratio of hole diameter to hole spacing.

Figure **4-20**A shows the pattern that was used for the *in vivo* robot application and

Figure **4-20**B was the pattern that would be used for this application.

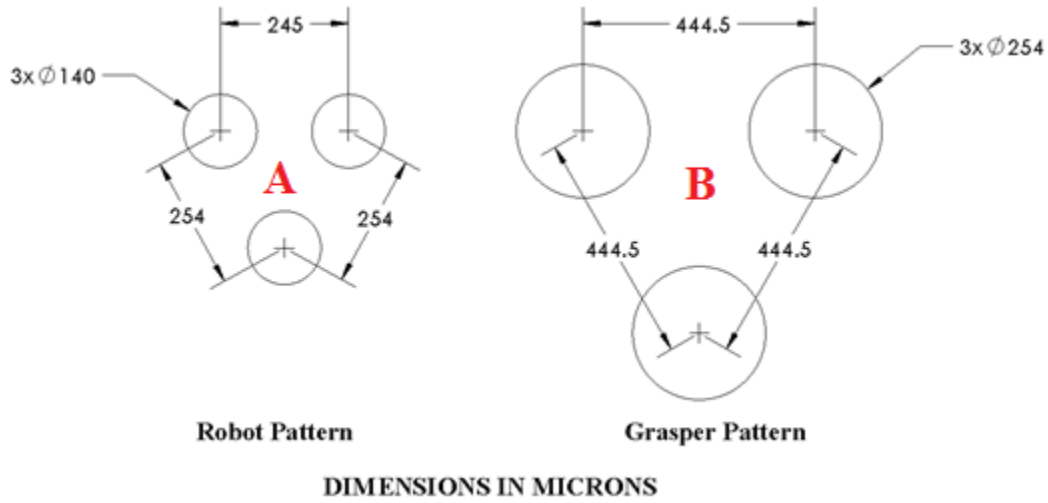

Figure 4-20 Mold Pattern for PDMS Tread for *In Vivo* Robot (A) and Grasper (B)

To make the mold an 89 x 12 mm piece of ¼" acrylic was cut out and three rectangles measuring 25 x 8 mm were repeatedly engraved to form three 0.5 mm deep recesses where the PDMS would be poured into. The hole pattern shown in

Figure 4-20 was cut into the recesses as shown in Figure 4-21. Sylgard® 184 Silicone Elastomer (Dow Corning, Midland MI), a two-part kit, was used to make the PDMS treads. One mL of the base material was mixed with 0.1 mL of the curing agent for a 10:1 mixing ratio. Once the two parts were thoroughly mixed and the air bubbles were removed, the liquid PDMS was poured into the acrylic mold and cured on a 75°C hot plate for 1 hour until the PDMS had fully cured.

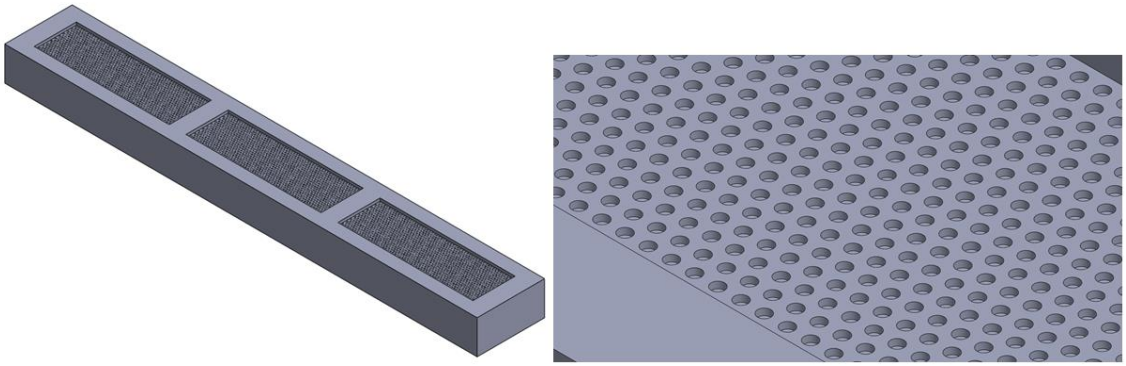

Figure 4-21 Acrylic Mold for PDMS Treads

After peeling the treads from the mold the frictional properties of the PDMS treads alone were tested. It was desired to see how much frictional force was generated between the treads and tissue for varying amounts of normal force. The range of normal forces tested remained under the 3.7 N maximum the compliant grasper was capable of producing. The testing setup can be seen in Figure 4-22. An 8 mm x 27 mm strip of tread was cut from the PDMS and adhered to a piece of 0.040" shim stock of the same dimension using transfer tape. A paper clip was partially straightened and glued to the top of the shim stock using Loctite 4014 instant adhesive. Pig liver samples 3 mm x 7 mm x 5 mm in size were placed under the treads and kept wet for the duration of testing. Weights were placed on top of the shim stock so the normal force was evenly distributed to the PDMS. Weight was then incrementally added below the pivot point to pull the PDMS to the point of a loss of grip.

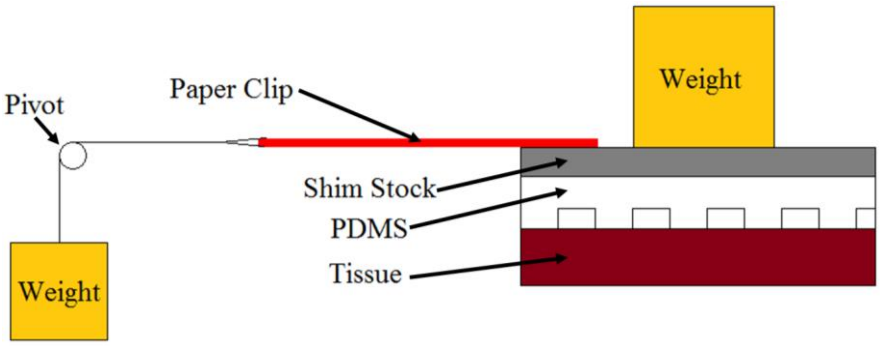

Figure 4-22 Traction Test Setup for PDMS Treads (not to scale)

Ten trials were performed at two different levels of normal force, 1.47 N and 1.76 N. In the trials of 1.47 N there was an immediate loss of grip in all ten trials when the minimum weight of 50 grams or 0.5 N was loaded. When the normal force was increased to 1.76 N the average maximum pull force was 0.9 N. Therefore it could be extrapolated that mounting the treads onto both jaws would give an average maximum pull force of approximately 3.78 N because the maximum pinch force the grasper is capable of producing is 3.7 N which is 2.1 times of the 1.76 N normal force, and which would then be multiplied by a factor of two since there would be two friction surfaces.

Strips of PDMS were then mounted onto the jaws using transfer adhesive (Figure 4-23) for traction improvement testing. The testing procedure from Section 4.5.2 was repeated. By adding the treads to the jaws the average maximum pull force barely increased to 1.5 N, which is about 40% of the theoretical pull force of 3.78N. This lack of traction increase could be attributed to a few factors. One being that there was a noticeable amount of tissue residue (“gunk”) on the treads after the previously mentioned traction testing. This may have prevented the treads from getting a good grip on the tissue surface due to the buildup in between the treads. Another factor was that the size of the

treads was too big. The pattern used in the mold for these treads was about 80% larger than one used in the *in vivo* robot application [4-13].

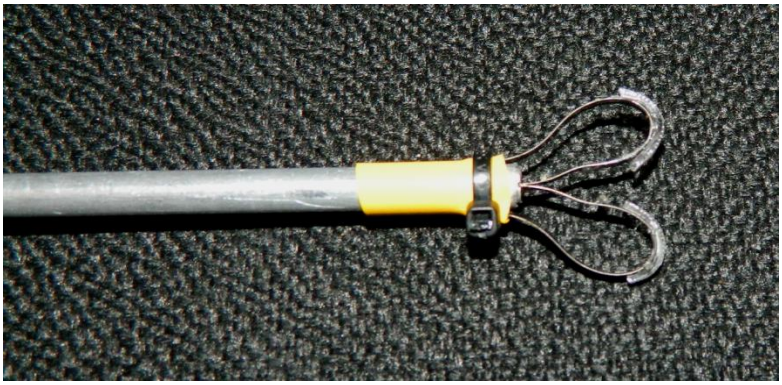

Figure 4-23 Jaws with PDMS treads

Further efforts were made to increase the pull force of the Nitinol jaws. As a proof-of-concept to illustrate the premise that adding a textured surface to the jaws would increase traction, 100-grit sandpaper was glued to the jaws with Loctite 4014 and pull tests were repeated using the same protocol outlined in Section 4.5.2. Ten trials were performed with an average pull force of 2.0 N which is close to the 2.5 N average pull force reported for laparoscopic grasper [4-10]. The last trial was not counted because the tissue slipped out of the jaws when the minimum load of 0.5 N was applied. This occurred because the sandpaper had built up a substantial amount of residue on its surface, reducing the traction between the jaws and the tissue. While some laparoscopic graspers do have teeth smaller than 1 mm teeth used in the AutoSuture™ Endoclinch™ II that was used for testing, they do not have the same issue of residue build up because the channels between the teeth are not irregular as they are in sandpaper. Having regular recesses in the teeth can allow the residue to be flushed out easily whereas the opposite is true for sandpaper. Future work could address other approaches to improve the traction

with teeth or tread sized on the order of the 100-grit sandpaper and using a material with a higher stiffness than PDMS for this application.

Chapter 5 Conclusions

This thesis presents two projects that involved the design, analysis, and testing of two grasping tools intended for two types of surgical procedures, NOTES and laparoscopic surgery. Both of these projects used superelastic Nitinol ribbon to allow large deformations and satisfy the goal of compliant grasping. The profile shape of the Nitinol was strongly linked to the grasping behavior in both applications. For the NOTES retainer assembly, simulation data led to the decision that a plateau shaped retainer proved better than a double-peak or single-peak shaped retainer because it displayed a stable grasping behavior with lower magnitudes of insertion forces. Trends in the clamping and insertion forces generated by the retainer were established to help identify regions of stable and unstable grasping and the geometric features that caused them. Qualitative testing was performed successfully, but to fully determine the success of the retainer design cooperative testing with the *in vivo* robots should be further pursued. Future work to improve the retainer design would include an optimization of the retainer shape to lower the insertion force needed to extract the payload from the retainer and meet the 1 N requirement.

Quantitative testing of the compliant laparoscopic grasper showed that an upper limit of applicable pinch force exists and that further closing of the jaws did not result in an increase in pinch force. By having a “built-in” maximum pinch force, a surgeon can fully squeeze the trigger of the grasper handle and not worry about applying excess force that can damage the tissue. Traction between the Nitinol jaws and tissue needed to be improved for the compliant grasper to become useful in a surgical setting and to reach the 5 N requirement. Micropatterned PDMS treads offered some traction improvement but

not enough to reach the desired levels and more appropriate methods of increasing the traction between the Nitinol jaws and soft tissue need to be explored. Additionally fatigue testing of the jaw should be performed to determine the risk level of the jaws fracturing under stress which could result in violent tissue laceration.

References

[2-1] Duerig, T., Pelton, A., & Stöckel, D. (1999). An overview of nitinol medical applications. Materials Science and Engineering: A, 273, 149-160.

[2-2] Stoeckel, D. (2000). Nitinol medical devices and implants. Minimally Invasive Therapy & Allied Technologies, 9(2), 81-88.

[2-3] Graesser, E. J., & Cozzarelli, F. A. (1991). Shape-memory alloys as new materials for aseismic isolation. Journal of Engineering Mechanics, 117(11), 2590-2608.

[2-4] De Lange, R. G., & Zijderveld, J. A. (1968). Shape-Memory Effect and the Martensitic Transformation of TiNi. Journal of Applied Physics, 39(5), 2195-2200.

[2-5] Pelton, A. R., Stöckel, D., & Duerig, T. W. (2000, January). Medical uses of nitinol. In Materials Science Forum (Vol. 327, pp. 63-70).

[2-6] Stoeckel, D., Pelton, A., & Duerig, T. (2004). Self-expanding nitinol stents: material and design considerations. European radiology, 14(2), 292-301.

[2-7] Civjan, S., Huget, E. F., & DeSimon, L. B. (1975). Potential applications of certain nickel-titanium (nitinol) alloys. Journal of dental research, 54(1), 89-96.

[2-8] Shabalovskaya, S. A. (2002). Surface, corrosion and biocompatibility aspects of Nitinol as an implant material. Bio-medical materials and engineering, 12(1), 69-109.

[2-9] Ratner, B. D. (2001). A perspective on titanium biocompatibility. In Titanium in medicine (pp. 1-12). Springer Berlin Heidelberg.

[2-10] Morgan, N. B. (2004). Medical shape memory alloy applications—the market and its products. Materials Science and Engineering: A, 378(1), 16-23.

[2-11] Callister Jr., W. D. (2007). Materials science and engineering: An introduction. (7th ed. ed., pp. 348-350). New York: John Wiley & Sons, Inc.

[2-12] Johnson Matthey Medical Components. How Does Nitinol Work? All About Nitinol Shape Memory and Superelasticity. http://jmmedical.com/resources/122/How-Does-Nitinol-Work%3F-All-About-Nitinol-Shape-Memory-and-Superelasticity.html. Accessed 3-20-2013.

[2-13] Barras, C. D. J., & Myers, K. A. (2000). Nitinol–its use in vascular surgery and other applications. European Journal of Vascular and Endovascular Surgery, 19(6), 564-569.

[2-14] Bishara, S. E., Barrett, R. D., & Selim, M. I. (1993). Biodegradation of orthodontic appliances. Part II. Changes in the blood level of nickel. American Journal of Orthodontics and Dentofacial Orthopedics, 103(2), 115-119.

[2-15] Prince, M. R., Salzman, E. W., Schoen, F. J., Palestrant, A. M., & Simon, M. (1988). Local intravascular effects of the nitinol wire blood clot filter. Investigative Radiology, 23(4), 294-300.

[2-16] Cragg, A. H., De Jong, S. C., Barnhart, W. H., Landas, S. K., & Smith, T. P. (1993). Nitinol intravascular stent: results of preclinical evaluation. Radiology, 189(3), 775-778.

[2-17] Zhao, S., Gu, L., & Froemming, S. R. (2011). Assessment of shape memory alloy stent deployment in a stenosed artery. Biomedical Engineering Letters, 1(4), 226-231.

[2-18] Rosenthal, D., Wellons, E. D., Levitt, A. B., Shuler, F. W., O'CONNER, R. E., & Henderson, V. J. (2004). Role of prophylactic temporary inferior vena cava filters placed at the ICU bedside under intravascular ultrasound guidance in patients with multiple trauma. Discussion. Journal of vascular surgery, 40(5), 958-964.

[2-19] Kourambas, J., Delvecchio, F. C., Munver, R., & Preminger, G. M. (2000). Nitinol stone retrieval-assisted ureteroscopic management of lower pole renal calculi. Urology, 56(6), 935.

[2-20] Electro Medical Systems. Lithobasket® Kit. http://www.ems-company.com/?plugin=cms&webpage_id=2305. Accessed 3/39/13

[3-1] ASGE and SAGES. 2006. ASGE/SAGES working group on natural orifice translumenal endoscopic surgery, white paper October 2005. Gastrointestinal Endoscopy, 63(2): 199-203.

[3-2] Midday, J. (2012). Material Handling System for Robotic Natural Orifice Surgery. Thesis.

[3-3] Lehman, A.C., Wood, N.A., Dumpert, J., Oleynikov, D., Farritor, S.M., 2008, "Dexterous Miniature in vivo Robot for NOTES," 2nd IEEE RAS & EMBS International Conference on Biomedical Robotics and Biomechatronics, 2008. BioRob 2008, pp.244-249.

[3-4] Hawks, J. A. (2010). Improved mobile wireless in vivo surgical robots: Modular design, expe6rimental results, and analysis. Thesis.

[3-5] Rentschler, M. E., Dumpert, J., Platt, S. R., Oleynikov, D., Farritor, S. M., & Iagnemma, K. (2006, May). Mobile in vivo biopsy robot. In Robotics and

Automation, 2006. ICRA 2006. Proceedings 2006 IEEE International Conference on (pp. 4155-4160). IEEE.

[3-6] LSTC. (2007). LS-DYNA Keyword User's Manual. (Version 971, p. 140 (MAT)).

[4-1] Westebring-van der Putten, E.P., van den Dobbelsteen, J.J., Goossens, R.H.M., Jakimowicz, J.J., Dankelman, J., 2009, "Effect of Laparoscopic Grasper Force Transmission Ratio on Grasp Control," Surgical Endoscopy, 23(47), 848-824.

[4-2] Heijnsdijk, E.A.M., deVisser, H., Dankelman, J., Gouma, D.J., 2004, "Slip and Damage Properties of Jaw of Laparoscopic Graspers," Surgical Endoscopy, 18(6), 974-979.

[4-3] Patterson, E. J., & Nagy, A. G. (1997). Don't cry over spilled stones? Complications of gallstones spilled during laparoscopic cholecystectomy: case report and literature review. Canadian journal of surgery, 40(4), 300-303.

[4-4] Cullis SN, Jeffery PC, McLauchlan G, Borman PC. Intraperitoneal abscess after laparoscopic cholecystectomy. Surg Laparosc Endosc 1992;2(4):337-8.

[4-5] Kraft K, Butters M, Bittner R: [The lost gallstone -- complication after laparoscopic cholecystectomy] [see comment]. Chirurg 1994;65(2):142-3. Comment in: Chirurg 1994;65(4):410

[4-6] Shakeshaft, A. J., Cartmill, J. A., Walsh, W. R., Martin, C. J., 2001, "A Curved Edge Moderates High Pressure Generated by a Laparoscopic Grasper," Surgical Endoscopy, 15(10), 1232-1234.

[4-7] Marucci, D. D., Cartmill, J. A., Martin, C. J. and Walsh, W. R., 2002, "A Compliant Tip Reduces the Peak Pressure of Laparoscopic Graspers," Australian and New Zealand Journal of Surgery, 72(7), 476–478.

[4-8] Cartmill, J. A., Shakeshaft, A. J., Walsh, W. R., & Martin, C. J. (1999). High pressures are generated at the tip of laparoscopic graspers. Australian and New Zealand journal of surgery, 69(2), 127-130.

[4-9] Schostek, S., Schuur, M.O., Buess, G.F., 2009, "Review on Aspects of Artificial Tactile Feedback in Laparoscopic Surgery," Journal of Medical Engineering & Physics, 31(8), 887-898.

[4-10] deVisser, H., Heijnsdijk, E.A.M., Herder, J.L., Pistecky, P.V., 2002, "Forces and Displacements in Colon Surgery", Surgical Endoscopy, 16(10), 1426-1430.

[4-11] Interlink Electronics . FSR® Force Sensing Resistor® Integration Guide and Evaluation Parts Catalog. http://resenv.media.mit.edu/classes/MAS836/Readings/fsrguide.pdf. Accessed 3-17-2013.

[4-12] Karagozler, M. E., Cheung, E., Kwon, J., & Sitti, M. (2006, February). Miniature endoscopic capsule robot using biomimetic micro-patterned adhesives. In Biomedical Robotics and Biomechatronics, 2006. BioRob 2006. The First IEEE/RAS-EMBS International Conference on (pp. 105-111). IEEE.[4-13] Sliker, L. J., Wang, X., Schoen, J. A., & Rentschler, M. E. (2010). Micropatterned treads for in vivo robotic mobility. *Journal of medical devices*,*4*(4).

[4-14] Lim, Dr. Jung Yul. Personal Interview. 27 February 2013.

[4-15] Epilog Laser. Owner's Manual for Epilog Mini/Helix – Model 8000. 22 April 2010. http://www.epiloglaser.com/downloads/pdf/mini_helix_4.22.10.pdf. Page 196.

Appendix A: Rejected Jaw Profiles

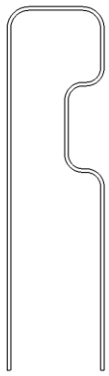

Poor – Jaws came together at a point instead of surface. Lots of stress in long segments.

Poor - Jaws came together at a point instead of surface.

Poor – Jaws came together at a point instead of surface.

Poor – Jaws came together at a point instead of surface

Poor – Jaws came together at a point instead of surface

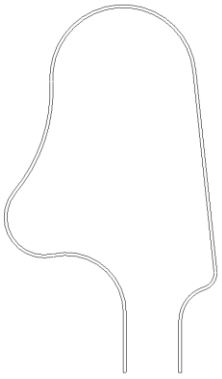

Poor – Jaws came together at a point instead of surface

Okay – Jaws came together at a point but eventually the contact surfaces came together

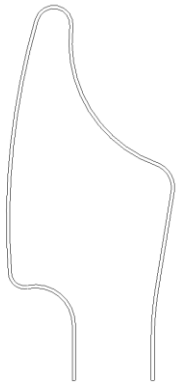

Better – Curved surface allowed jaws to come together at surface but jaws contracted (shortened in length)

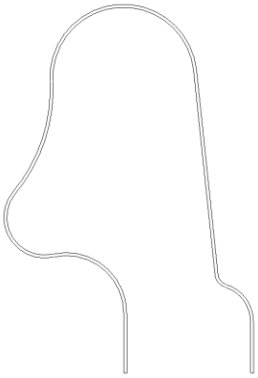

Poor - Jaw came together at a point instead of surface

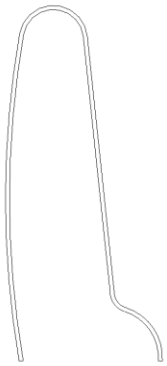

Poor - Jaw came together at a point instead of surface

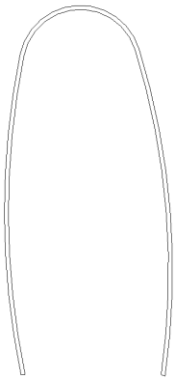

Poor – Jaw contracted significantly.

Okay – Jaws met at contact surface but contraction was still present

Better - Jaw came together at surface but double-actuation would be needed to open and close jaws

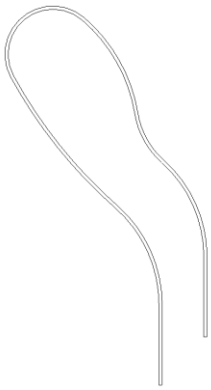

Best – Allowed single action actuation, jaws came together at surface, and little to no contraction was present

Appendix B: LabVIEW VI

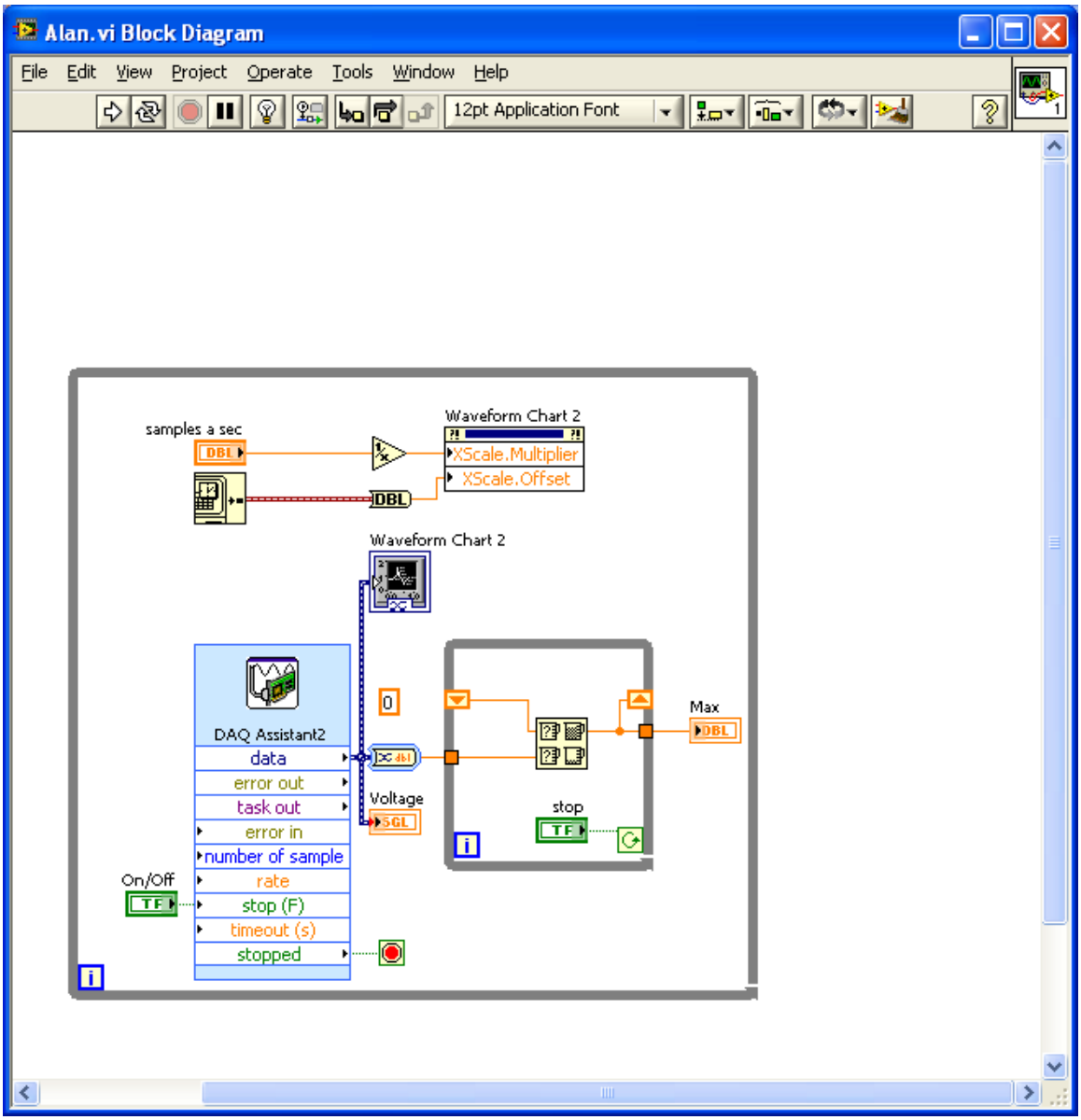

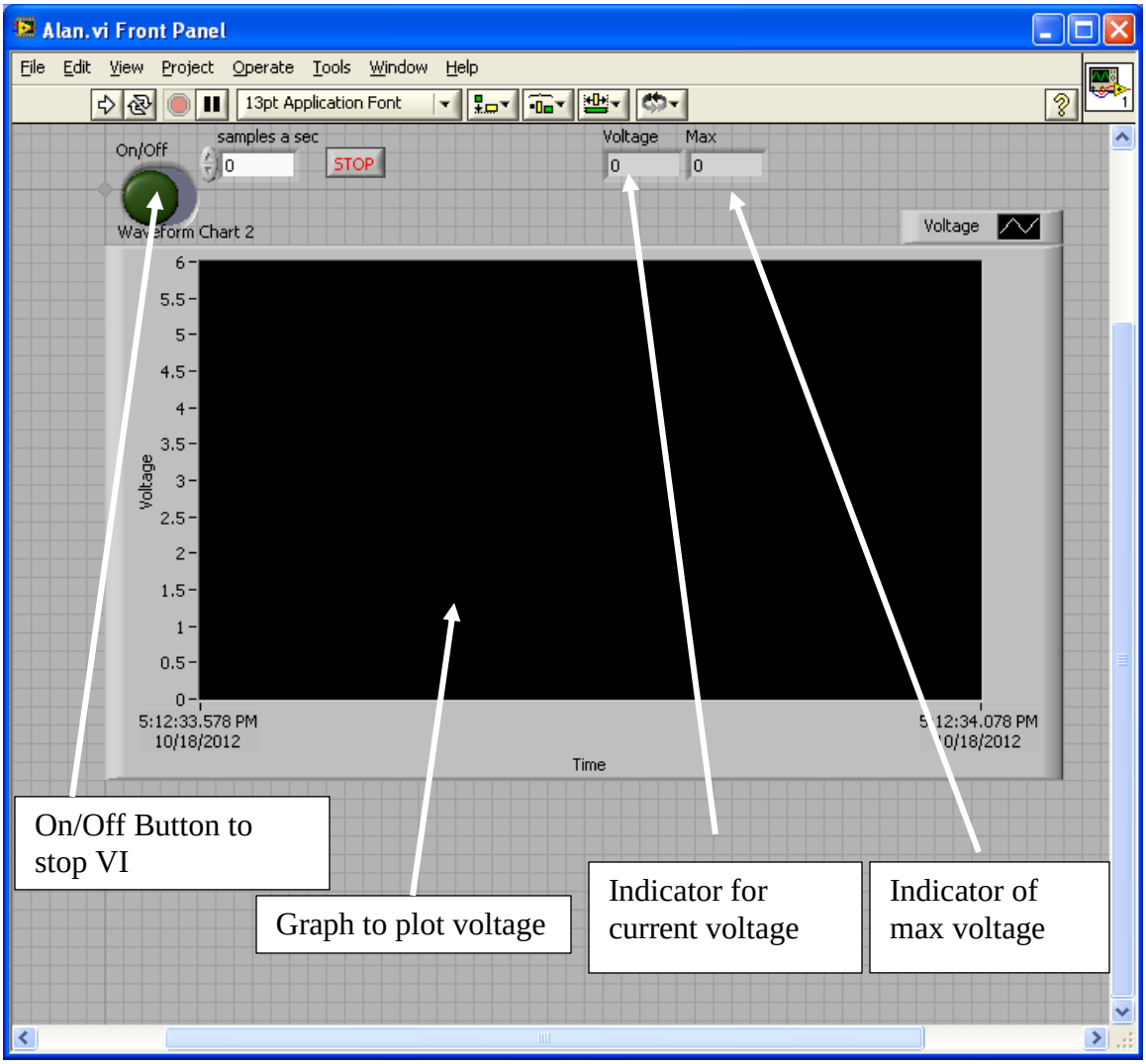
Alan.vi Front Panel
File Edit View Project Operate Tools Window Help
13pt Application Font
On/Off
samples a sec
0
STOP
Voltage
Max
0
0
Waveform Chart 2
Voltage
6
5.5
5
4.5
4
3.5
3
2.5
2
1.5
1
0.5
0
Voltage
5:12:33.578 PM
10/18/2012
Time
On/Off Button to stop VI
Graph to plot voltage
Indicator for current voltage
Indicator of max voltage

National Semiconductor

August 2000

LM124/LM224/LM324/LM2902
Low Power Quad Operational Amplifiers

General Description

The LM124 series consists of four independent, high gain, internally frequency compensated operational amplifiers which were designed specifically to operate from a single power supply over a wide range of voltages. Operation from split power supplies is also possible and the low power supply current drain is independent of the magnitude of the power supply voltage.

Application areas include transducer amplifiers, DC gain blocks and all the conventional op amp circuits which now can be more easily implemented in single power supply systems. For example, the LM124 series can be directly operated off of the standard +5V power supply voltage which is used in digital systems and will easily provide the required interface electronics without requiring the additional ±15V power supplies.

Unique Characteristics

- In the linear mode the input common-mode voltage range includes ground and the output voltage can also swing to ground, even though operated from only a single power supply voltage
- The unity gain cross frequency is temperature compensated
- The input bias current is also temperature compensated

Advantages

- Eliminates need for dual supplies
- Four internally compensated op amps in a single package
- Allows directly sensing near GND and V_{OUT} also goes to GND
- Compatible with all forms of logic
- Power drain suitable for battery operation

Features

- Internally frequency compensated for unity gain
- Large DC voltage gain 100 dB
- Wide bandwidth (unity gain) 1 MHz (temperature compensated)
- Wide power supply range:
  Single supply 3V to 32V
  or dual supplies ±1.5V to ±16V
- Very low supply current drain (700 µA)—essentially independent of supply voltage
- Low input biasing current 45 nA (temperature compensated)
- Low input offset voltage 2 mV and offset current: 5 nA
- Input common-mode voltage range includes ground
- Differential input voltage range equal to the power supply voltage
- Large output voltage swing 0V to V+ − 1.5V

Connection Diagram

Dual-In-Line Package

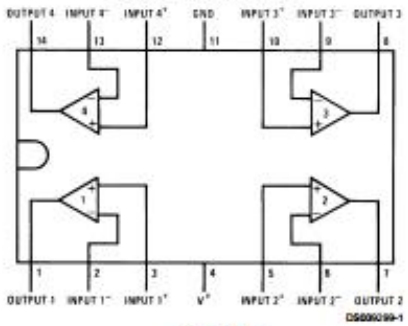

Top View

Order Number LM124J, LM124AJ, LM124J/883 (Note 2), **LM124AJ/883** (Note 1), **LM224J, LM224AJ, LM324J, LM324M, LM324MX, LM324AM, LM324AMX, LM2902M, LM2902MX, LM324N, LM324AN, LM324MT, LM324MTX or LM2902N LM124AJRQML and LM124AJRQMLV**(Note 3)

See NS Package Number J14A, M14A or N14A

Note 1: LM124A available per JM38510/11006

Note 2: LM124 available per JM38510/11005

Appendix C: Grasper Testing Raw Data

Pinch Force Data:

Compliant

Disp [mm]	Voltage [V]		
3	0.4	0.5	0.6
4	0.6	0.9	0.7
5	0.8	0.9	0.8
6	1	1	1.1
7	1.2	1.2	1.3
8	1.45	1.8	1.6
9	2.4	2.2	
10	2.7	2.5	
11	2.8	2.5	
12	2.8	2.5	
13	2.8	2.5	
12	2.6	2.4	
11	2.6	2.6	
10	2.7	2.4	
9	2.3	2.2	
8	1.1	1.7	
7	1.3	0.6	
6	1.1	0.9	
5	0.7	0.8	
4	0.7	0.9	
3	0.5	0.7	

Disp [mm]	Avg. Voltage	Avg. Pinch Force [N]
3	0.5	0.63
4	0.8	0.95
5	0.8	1.01
6	1.0	1.32
7	1.1	1.47
8	1.5	2.06
9	2.3	3.13
10	2.6	3.57
11	2.6	3.64
12	2.6	3.57
13	2.7	3.67

Rigid

	Voltage [V]	Pinch Force [N]
	4.7	9.4
	4.5	8.9
	4.5	8.9
	4.4	8.6
	4.4	8.6
	4.4	8.6
	4.4	8.6
	4.3	8.4
	4.3	8.4
	4.4	8.6
Average	4.43	8.7
Std. Dev.	0.11	0.3

Pull Force Data:

Compliant

	Force [N]
	1.7
	0.9
	1.2
	2.0
	1.1
	1.5
	1.1
	2.0
	0.8
	0.9
	1.2
	0.8
	2.9
Average	1.4
Std. Dev.	0.6

Rigid

Force [N]	
7.4	
8.8	
9.8	
7.4	
7.4	
7.6	
8.6	
7.6	
8.3	
8.1	Average
0.8	Std. Dev.

Appendix D: Reduced LS-DYNA Code

```
*KEYWORD
*TITLE
NOTES Retainer
$$$$$$$$$$$$$$$$$$$$$$$$$$$$$$$$$$$$$$$$$$$$$$$$$$$$$$$$$$$$$$$$$$$$$$$$$$$$$$$$$$$$$$$$$$$
$
$ NOTES Retainer Project
$ Alan Goyzueta
$ Created 2/14/13
$$$$$$$$$$$$$$$$$$$$$$$$$$$$$$$$$$$$$$$$$$$$$$$$$$$$$$$$$$$$$$$$$$$$$$$$$$$$$$$$$$$$$$$$$$$
$
$
$ Units: mm, ms, gm, N, N-mm, MPa
$
$$$$$$$$$$$$$$$$$$$$$$$$$$$$$$$$$$$$$$$$$$$$$$$$$$$$$$$$$$$$$$$$$$$$$$$$$$$$$$$$$$$$$$$$$$$
$
$
$ Three retainer pairs with different profile shapes: plateau, double-peak, and single-
$peak
$ Retainers have fixed-free boundary conditions
$ 3 mm pin passed through retainer assembly at 0.2 mm/ms
$ Pin constrained to 2 DOFs (Y & Z translation)
$
$$$$$$$$$$$$$$$$$$$$$$$$$$$$$$$$$$$$$$$$$$$$$$$$$$$$$$$$$$$$$$$$$$$$$$$$$$$$$$$$$$$$$$$$$$$
$
$
$$$$  Control Ouput
$
$$$$$$$$$$$$$$$$$$$$$$$$$$$$$$$$$$$$$$$$$$$$$$$$$$$$$$$$$$$$$$$$$$$$$$$$$$$$$$$$$$$$$$$$$$$
$
$
*CONTROL_HOURGLASS
$      ihq        qh
         4      0.03
$
*CONTROL_ENERGY
$     hgen      rwen    slnten     rylen
         2         2         2         1
$
*CONTROL_OUTPUT
$    npopt    neecho    nrefup    iaccop     opifs    ipnint    ikedit    iflush
         1         3                                               100      5000
$    iprtf    ierode     tet10    msgmax    ipcurv
                             2        50
$
*CONTROL_SHELL
$   wrpang     esort     irnxx    istupd    theory       bwc     miter      proj
      20.0                  -1                   2         1         1         1
$  rotascl    intgrd    lamsht    cstyp6    tshell    nfail1    nfail4   psnfail
       1.0                               1
$  psstupd    irquad     cntco    itsflg    irquad
                                                 2
$
*CONTROL_TERMINATION
$   endtim    endcyc     dtmin    endeng    endmas
     100.0
$
$
$$$$$$$$$$$$$$$$$$$$$$$$$$$$$$$$$$$$$$$$$$$$$$$$$$$$$$$$$$$$$$$$$$$$$$$$$$$$$$$$$$$$$$$$$$$
$
$
$$$$  Database Files
$
$$$$$$$$$$$$$$$$$$$$$$$$$$$$$$$$$$$$$$$$$$$$$$$$$$$$$$$$$$$$$$$$$$$$$$$$$$$$$$$$$$$$$$$$$$$
$
$
*DATABASE_GLSTAT
$       dt
```

```
  0.100000
$
*DATABASE_MATSUM
$       dt
  0.100000
$
*DATABASE_NODOUT
$       dt
  0.100000
$
*DATABASE_HISTORY_NODE
$      id1       id2       id3       id4       id5       id6       id7       id8
     81230
$
*DATABASE_RCFORC
$       dt
  0.100000
$
*DATABASE_RWFORC
$       dt
  0.100000
$
*DATABASE_BINARY_D3PLOT
$       dt
  5.000000
$

$
*DATABASE_EXTENT_BINARY
$    neiph     neips    maxint    strflg    sigflg    epsflg    rltflg    engflg
                             3                   1         1         1         1
$   cmpflg    ieverp    beamip     dcomp      shge     stssz    n3thdt   ialemat
                   1                   1         1         1         2         1
$  nintsld   pkp_sen      sclp    unused     msscl     therm    intout    nodout
                      1.000000                                  STRESS    STRESS
$     dtdt    resplt

$
$$$$$$$$$$$$$$$$$$$$$$$$$$$$$$$$$$$$$$$$$$$$$$$$$$$$$$$$$$$$$$$$$$$$$$$$$$$$$$$$$$$$$$$$$$$$
$
$
$$$$  Define Contact - Automatic Single Surface Contact
$$$$$  - Force Transducers Between Pin and Retainer (6 total)
$
$$$$$$$$$$$$$$$$$$$$$$$$$$$$$$$$$$$$$$$$$$$$$$$$$$$$$$$$$$$$$$$$$$$$$$$$$$$$$$$$$$$$$$$$$$$$$
$
$
*CONTACT_AUTOMATIC_SINGLE_SURFACE
$     ssid      msid     sstyp     mstyp    sboxid    mboxid       spr       mpr
         0
$       fs        fd        dc        vc       vdc    penchk        bt        dt
      0.08      0.08                                                  1.0000E+20
$      sfs       sfm       sst       mst      sfst      sfmt       fsf       vsf
       1.0       1.0                 0.5       1.0       1.0       1.0       1.0
$
*CONTACT_FORCE_TRANSDUCER_ID
$      cid                                                                  title
         2Plateau1
$     ssid      msid     sstyp     mstyp    sboxid    mboxid       spr       mpr
         7         1         3         3
$       fs        fd        dc        vc       vdc    penchk        bt        dt
      0.08      0.08                                                  1.0000E+20
$      sfs       sfm       sst       mst      sfst      sfmt       fsf       vsf
       1.0       1.0                           1.0       1.0       1.0       1.0
$
*CONTACT_FORCE_TRANSDUCER_ID
$      cid                                                                  title
         3Plateau2
$     ssid      msid     sstyp     mstyp    sboxid    mboxid       spr       mpr
         7         2         3         3
$       fs        fd        dc        vc       vdc    penchk        bt        dt
```

```
     0.08      0.08                                                   1.0000E+20
$     sfs       sfm       sst       mst      sfst      sfmt       fsf       vsf
      1.0       1.0                           1.0       1.0       1.0       1.0
$
*CONTACT_FORCE_TRANSDUCER_ID
$     cid                                                                 title
        4Double1
$    ssid      msid     sstyp     mstyp    sboxid    mboxid       spr       mpr
        8         3         3         3
$      fs        fd        dc        vc       vdc    penchk        bt        dt
     0.08      0.08                                                   1.0000E+20
$     sfs       sfm       sst       mst      sfst      sfmt       fsf       vsf
      1.0       1.0                           1.0       1.0       1.0       1.0
$
*CONTACT_FORCE_TRANSDUCER_ID
$     cid                                                                 title
        5Double2
$    ssid      msid     sstyp     mstyp    sboxid    mboxid       spr       mpr
        8         4         3         3
$      fs        fd        dc        vc       vdc    penchk        bt        dt
     0.08      0.08                                                   1.0000E+20
$     sfs       sfm       sst       mst      sfst      sfmt       fsf       vsf
      1.0       1.0                           1.0       1.0       1.0       1.0
$
*CONTACT_FORCE_TRANSDUCER_ID
$     cid                                                                 title
        6Single1
$    ssid      msid     sstyp     mstyp    sboxid    mboxid       spr       mpr
        9         5         3         3
$      fs        fd        dc        vc       vdc    penchk        bt        dt
     0.08      0.08                                                   1.0000E+20
$     sfs       sfm       sst       mst      sfst      sfmt       fsf       vsf
      1.0       1.0                           1.0       1.0       1.0       1.0
$
*CONTACT_FORCE_TRANSDUCER_ID
$     cid                                                                 title
        7Single2
$    ssid      msid     sstyp     mstyp    sboxid    mboxid       spr       mpr
        9         6         3         3
$      fs        fd        dc        vc       vdc    penchk        bt        dt
     0.08      0.08                                                   1.0000E+20
$     sfs       sfm       sst       mst      sfst      sfmt       fsf       vsf
      1.0       1.0                           1.0       1.0       1.0       1.0
$
$$$$$$$$$$$$$$$$$$$$$$$$$$$$$$$$$$$$$$$$$$$$$$$$$$$$$$$$$$$$$$$$$$$$$$$$$$$$$$$$$$$$$$$$$$$
$
$
$$$$  Prescribed Motion to Pin
$
$$$$$$$$$$$$$$$$$$$$$$$$$$$$$$$$$$$$$$$$$$$$$$$$$$$$$$$$$$$$$$$$$$$$$$$$$$$$$$$$$$$$$$$$$$$
$
$
*BOUNDARY_PRESCRIBED_MOTION_SET
$    nsid       dof       vad      lcid        sf       vid     death     birth
        2         2         0         1       1.0          1.0000E+28
$
*DEFINE_CURVE
$    lcid      sidr       sfa       sfo      offa      offo
        1                 1.0       1.0
$                a1                  o1
                  0                 0.2
        1.0e+008                    0.2
$
$$$$$$$$$$$$$$$$$$$$$$$$$$$$$$$$$$$$$$$$$$$$$$$$$$$$$$$$$$$$$$$$$$$$$$$$$$$$$$$$$$$$$$$$$$$
$
$
$$$$  Define Boundary Conditions
$
$$$$$$$$$$$$$$$$$$$$$$$$$$$$$$$$$$$$$$$$$$$$$$$$$$$$$$$$$$$$$$$$$$$$$$$$$$$$$$$$$$$$$$$$$$$
$
$
```

```
$$$$$$$$$$$$$$$$$$$$$$$$$$$$$$$$$$$$$$$
$$$ Fix Retainer End
$$$$$$$$$$$$$$$$$$$$$$$$$$$$$$$$$$$$$$$
$
*BOUNDARY_SPC_SET
$     nsid       cid      dofx      dofy      dofz     dofrx     dofry     dofrz
         1                   1         1         1         1         1         1
$
$$$$$$$$$$$$$$$$$$$$$$$$$$$$$$$$$$$$$$$
$$$$ Constrain Pin to 2 DOFs
$$$$$$$$$$$$$$$$$$$$$$$$$$$$$$$$$$$$$$$
$
*BOUNDARY_SPC_SET
$     nsid       cid      dofx      dofy      dofz     dofrx     dofry     dofrz
         2                   1         0         0         1         1         1
$
$$$$$$$$$$$$$$$$$$$$$$$$$$$$$$$$$$$$$$$$$$$$$$$$$$$$$$$$$$$$$$$$$$$$$$$$$$$$$$$$$$$$$$$$$$$$$$
$
$
$$$$  Define Rigidwall
$
$$$$$$$$$$$$$$$$$$$$$$$$$$$$$$$$$$$$$$$$$$$$$$$$$$$$$$$$$$$$$$$$$$$$$$$$$$$$$$$$$$$$$$$$$$$$$$
$
$
*RIGIDWALL_PLANAR_FORCES
$     nsid    nsidex     boxid    offset     birth     death     rwksf
         0                                        1.0000E+20  1.000000
$       xt        yt        zt        xh        yh        zh      fric      wvel
         0         0    -0.001         0         0         1      0.08
$

$
*RIGIDWALL_PLANAR_FORCES
$     nsid    nsidex     boxid    offset     birth     death     rwksf
         0                                        1.0000E+20  1.000000
$       xt        yt        zt        xh        yh        zh      fric      wvel
         0         0     8.739         0         0         0      0.08
$

$
$$$$$$$$$$$$$$$$$$$$$$$$$$$$$$$$$$$$$$$$$$$$$$$$$$$$$$$$$$$$$$$$$$$$$$$$$$$$$$$$$$$$$$$$$$$$$$
$
$
$$$$  Define Parts, Materials, Sections
$
$$$$$$$$$$$$$$$$$$$$$$$$$$$$$$$$$$$$$$$$$$$$$$$$$$$$$$$$$$$$$$$$$$$$$$$$$$$$$$$$$$$$$$$$$$$$$$
$
$
*PART
$  title
$      pid     secid       mid
$$
s1.1
         1         1         1
s1.2
         2         1         1
s2.1
         3         1         1
s2.2
         4         1         1
s3.1
         5         1         1
s3.2
         6         1         1
pin1
         7         2         2
pin2
         8         2         2
pin3
         9         2         2
$
```

```
*SECTION_SHELL
$    secid    elform      shrf       nip     propt   qr/irid     icomp     setyp
         1         2     0.833         4         1                             1
$       t1        t2        t3        t4
       0.2       0.2       0.2       0.2
$
*SECTION_SHELL
$    secid    elform      shrf       nip     propt   qr/irid     icomp     setyp
         2         2     0.833         4         1                             1
$       t1        t2        t3        t4
       0.5       0.5       0.5       0.5
$
*MAT_SHAPE_MEMORY
$      mid        ro         e        pr
         1   0.00645     24862       0.3
$  sig_ass   sig_asf   sig_sas   sig_saf      epsl     alpha      ymrt
       440       574       280       161     0.052
$
*MAT_ELASTIC
$      mid        ro         e        pr
         2     0.008   1.90E+5     0.305
$
$
```

Appendix E: Reduced ABAQUS Code

```
*Heading
** Job name: 2D_Compliant_Grasper_Open_No_Tissue Model name: 2D Compliant Grasper Open No
Tissue
** Generated by: Abaqus/CAE 6.9-2
*Preprint, echo=NO, model=NO, history=NO, contact=NO
**
** PARTS
**
*Part, name="Compliant Jaw"

[Define nodes and elements]

*Nset, nset=_PickedSet22, internal, generate
     1,  16184,      1
*Elset, elset=_PickedSet22, internal, generate
     1,  14154,      1
** Section: NiTI Section
*Solid Section, elset=_PickedSet22, material=REPLACEME
,
*End Part
**
*Part, name="Compliant Jaw_2"
*Node

[Define Nodes and Elements]

*Nset, nset=_PickedSet17, internal, generate
     1,  16184,      1
*Elset, elset=_PickedSet17, internal, generate
     1,  14154,      1
** Section: NiTI Section
*Solid Section, elset=_PickedSet17, material=REPLACEME
,
*End Part
**
**
** ASSEMBLY
**
*Assembly, name=Assembly
**
*Instance, name="Compliant Jaw-1", part="Compliant Jaw"
    0.001334,           0.,           0.
*End Instance
**
*Instance, name="Compliant Jaw_2-1", part="Compliant Jaw_2"
0.00138398421841959,           0.,           0.
*End Instance
**
*Nset, nset=_PickedSet491, internal, instance="Compliant Jaw-1"

[Define Node Set]

**
** MATERIALS
**
*Material, name=ABQ_SUPER_ELASTIC_1
*USER MATERIAL, CONSTANTS=15
24862233044., 0.3, 15595916743., 0.3, 0.052, 6.700000, 440000000., 574000000.,
22., 6.7, 280000000., 161000000.,,,0,
*depvar
24,
*Material, name=Rubber
*Density
1100.,
*Elastic
 5.5e+07, 0.5
**
```

```
** INTERACTION PROPERTIES
**
*Surface Interaction, name=IntProp-1
1.,
*Friction
0.,
*Surface Behavior, pressure-overclosure=HARD
**
** BOUNDARY CONDITIONS
**
** Name: Fix Type: Displacement/Rotation
*Boundary
_PickedSet490, 1, 1
_PickedSet490, 2, 2
**
** INTERACTIONS
**
** Interaction: Int-1
*Contact Pair, interaction=IntProp-1, type=SURFACE TO SURFACE, no thickness
_PickedSurf489, _PickedSurf488
** Interaction: Int-2
*Contact Pair, interaction=IntProp-1, type=SURFACE TO SURFACE
_PickedSurf493, _PickedSurf494
** Interaction: Int-3
*Contact Pair, interaction=IntProp-1, type=SURFACE TO SURFACE
_PickedSurf496, _PickedSurf497
** ----------------------------------------------------------------
**
** STEP: Step-1
**
*Step, name=Step-1, inc=10000
*Static
0.005, 1., 1e-07, 0.005
**
** BOUNDARY CONDITIONS
**
** Name: Push/Pull Type: Displacement/Rotation
*Boundary
_PickedSet491, 1, 1
_PickedSet491, 2, 2, -0.009
**
** OUTPUT REQUESTS
**
*Restart, write, frequency=0
**
** FIELD OUTPUT: F-Output-1
**
*Output, field
*Node Output
CF, RF, U
*Element Output, directions=YES
E, LE, S
*Contact Output
CDISP, CSTRESS
**
** HISTORY OUTPUT: H-Output-1
**
*Output, history, variable=PRESELECT
*End Step
```

Appendix F: Detailed Drawing of Final Compliant Jaw